

Lunar Outgassing, Transient Phenomena & the Return to the Moon

II: Predictions and Tests for Outgassing/Regolith Interactions

Arlin P.S. Crotts and Cameron Hummels

*Department of Astronomy, Columbia University, Columbia Astrophysics Laboratory,
550 West 120th Street, New York, NY 10027*

ABSTRACT

We follow Paper I with predictions of how gas leaking through the lunar surface could influence the regolith, as might be observed via optical Transient Lunar Phenomena (TLPs) and related effects. We touch on several processes, but concentrate on low and high flow rate extremes, perhaps the most likely. We model explosive outgassing for the smallest gas overpressure at the regolith base that releases the regolith plug above it. This disturbance's timescale and affected area are consistent with observed TLPs; we also discuss other effects.

For slow flow, escape through the regolith is prolonged by low diffusivity. Water, found recently in deep magma samples, is unique among candidate volatiles, capable of freezing between the regolith base and surface, especially near the lunar poles. For major outgassing sites, we consider the possible accumulation of water ice. Over geological time ice accumulation can evolve downward through the regolith. Depending on gases additional to water, regolith diffusivity might be suppressed chemically, blocking seepage and forcing the ice zone to expand to larger areas, up to km^2 scales.

We propose an empirical path forward, wherein current and forthcoming technologies provides controlled, sensitive probes of outgassing. The optical transient/outgassing connection, addressed via Earth-based remote sensing, suggests imaging and/or spectroscopy, but aspects of lunar outgassing might be more covert, as indicated above. TLPs betray some outgassing, but does outgassing necessarily produces TLPs? We also suggest more intrusive techniques from radar to in-situ probes. Understanding lunar volatiles seems promising in terms of resource exploitation for human exploration of the Moon and beyond, and offer interesting scientific goals in its own right, but many of these approaches should be practiced in a pristine lunar atmosphere, before significant confusing signals likely dominate when humans return to the Moon.

1. Introduction

Transient lunar phenomena (TLPs or LTPs) are defined for the purposes of this investigation as localized (smaller than a few hundred km across), transient (up to a few hours duration, and probably longer than typical impact events - less than 1s to a few seconds), and presumably confined to processes near the lunar surface. How such events are manifest is summarized by Cameron (1972). In Paper I (Crotts 2008; see also Crotts 2009) we study the systematic behavior (especially the spatial distribution) of TLP observations - particularly their significant correlations with tracers of lunar surface outgassing, and we are thereby motivated to understand if this correlation is directly causal.

Numerous works have offered hypotheses for the physical cause of TLPs (Mills 1970, Garlick et al. 1972a, b, Geake & Mills 1977, Cameron 1977, Middlehurst 1977, Hughes 1980, Robinson 1986, Zito 1989, Carbognani 2004, Davis 2009), but we present a methodical examination of the influence of outgassing, exploring quantitatively how outgassing might produce TLPs. Furthermore, it seems likely that outgassing activity is concentrated in several areas, which leads one to ask how outgassing might interact and alter the regolith presumably overlying the source of gas. Reviews of similar processes have been written, but few since the integration of Apollo-era data e.g., Stern (1999), Mukherjee (1975), Friesen (1975).

Several experiments from the Apollo missions indicate that gas is produced in the vicinity of the Moon, even though these experiments disagree on the total rate: 1) LACE (Lunar Atmosphere Composition Experiment on *Apollo 17*), $\sim 0.1 \text{ g s}^{-1}$ over the entire lunar surface (Hodges et al. 1973, 1974); 2) SIDE (Suprathermal Ion Detector Experiment on *Apollo 12*, *14*, *15*), $\sim 7 \text{ g s}^{-1}$ (Vondrak et al. 1974); 3) CCGE (Cold Cathode Gauge Experiment on *Apollo 12*, *14*, *15*), $\lesssim 60 \text{ g s}^{-1}$ (Hodges et al. 1972). These measurements not only vary by more than two orders of magnitude but in assayed species and detection methods. LACE results here applies only to neutral ^{40}Ar , ^{36}Ar and ^{20}Ne . By mass ^{40}Ar predominates. SIDE results all relate to ions, and perhaps include a large contribution from molecular species (Vondrak et al. 1974). CCGE measures only neutral species, and cannot easily distinguish between them.

The LACE data indicates episodic outgassing of ^{40}Ar on timescale of a few months or less (Hodges & Hoffman 1975), but resolving this into faster timescales is more ambiguous. In this discussion we adopt the intermediate rate (SIDE), about 200 tonne y^{-1} for the total production of gas, of all species, ionized or neutral. The LACE is the only instrument to provide compositional ratios, which in detail also include additional, rarer components. We will use these ratios and in some cases normalize them against the SIDE total.

Much of the following discussion is only marginally sensitive to the actual composition of

the gas. For many components of molecular gas at the lunar surface, however, there is a significant possible contribution from cometary or meteoritic impacts, and a lesser amount from solar wind/regolith interactions. The influx of molecular gas from comets and meteorites are variously estimated, usually in the range of tonnes or tens of tonnes per year over the lunar surface (see Anders et al. 1973, Morgan & Shemansky 1991). Cometary contributions may be sporadically greater (Thomas 1974). Except for H_2 , solar wind interactions (Mukherjee 1975) provide only a small fraction of the molecular concentration seen at the surface (which are only marginally detected: Hoffman & Hodges 1975). There is still uncertainty as to what fraction of this gas is endogenous. Current data do not succeed in resolving these questions, but we will return to consider them later in the context of gas seepage/regolith interactions.

In this paper we consider various effects of outgassing through the regolith (§2), and find the most interesting simple effect occurs when the flow is high enough to cause disruption of the regolith to relieve pressure (§3), which we compare to fluidization. Another interesting effect occurs when the gas undergoes a phase change while passing through the regolith (§4), which seems to apply primarily to water vapor. These effects suggest a variety of observational/experimental approaches, which we summarize in §5 and Appendix II.

2. Possible Modes of Outgassing/Regolith Interaction

One can easily picture several modes in which outgassing volatiles might interact with regolith on the way to the surface. These modes will come into play with increasing gas flow rate (and/or varies the regolith overburden), and we simply list them with mnemonic labels along with a description:

- 1) choke: complete blockage below the regolith, meaning that any chemistry or phase changes occur within the bedrock/megaregolith,
- 2) seep: gas is introduced slowly into the regolith, essentially molecule by molecule,
- 3) bubble: gas is introduced in macroscopic packets which stir or otherwise rearrange the regolith (such as “fluidization” e.g., Mills 1969),
- 4) gulp: gas is introduced in packets whose adiabatic expansion deposits kinetic energy into regolith and cools the gas, which therefore might even undergo a phase change,
- 5) explode: gas is deposited in packets at base of the regolith leading to an explosion, and
- 6) jet: there is little or no entrained material and gas simply flows into the vacuum at nearly the speed of sound.

While the intermediate processes might prove interesting, the extreme cases are probably more likely to be in effect and will receive more of our attention. In fact choking behavior might lead to explosions or geysers, when the pressure blockage is released. Since these latter two processes involve primarily simple hydrodynamics (and eventually, newtonian ballistics), we will consider them first, and how they might relate to TLPs.

3. Explosive Outgassing

If outgassing occurs at a rate faster than simple percolation can sustain, and where regolith obstructs its path to the surface, the accumulation of the gas will disrupt and cause bulk motion of the intervening regolith. The outgassing can lift the regolith into a cloud in the temporary atmosphere caused by the event. The presence of such a cloud has the potential to increase the local albedo from the perspective of an outside observer due to increased reflectivity and possible Mie scattering of underlying regolith. Additionally, volatiles buried in the regolith layer could become entrained in this gas further changing the reflective properties of such a cloud. Garlick et al. (1972b) describe fluidization of lunar regolith, in which dust is displaced only temporarily and/or over small distances compared to ballistic trajectories, but we will assume that we are dealing with more rapid changes.

3.1. Model Explosion

Let us construct a simple model of explosive outgassing through the lunar surface. For such an event to occur, we assume a pocket of pressurized gas builds at the base of the regolith, where it is delivered by transport through the crust/megaregolith presumably via channels or cracks, or at least faster diffusion from below. Given a sufficient flow rate (which we consider below), gas will accumulate at this depth until its internal pressure is sufficient to displace the overlying regolith mass, or some event releases downward pressure e.g., impact, moonquake, incipient fluidization, puncturing a seal, etc. We can estimate the minimal amount of gas alone required to cause explosive outgassing by assuming that the internal energy of the buried gas is equal to the total energy necessary to raise the overlying cone of regolith to the surface. This “minimal TLP” is the smallest outgassing event likely to produce potentially observable disruption at a new site, although re-eruption through thinned regolith will require less gas.

For the initial conditions of the first phase of our model, we assume the gas builds up at the base of the regolith layer at a depth of 15 m (for more discussion of this depth, see section 4). We set the bulk density of the regolith at 1.9 g cm^{-3} (McKay et al. 1991), thereby

setting the pressure at this depth at 0.45 atm. Because of the violent nature of an explosive outgassing, we assume that the cone of dust displaced will be 45° from vertical (comparable to the angle of repose for a disturbed slope of this depth: Carrier, Olhoeft & Mendell 1991). The mass of overlying regolith defined by this cone is $m = 7 \times 10^6$ kg.

In order to determine the mass of gas required to displace this regolith cone, we equate the internal energy of this gas bubble with the potential energy ($U = mgh$, where $g = 1.62$ m s $^{-2}$) required to lift the cone of regolith a height $h = 15$ m to the surface, requiring 47,000 moles of gas. Much of gas found in outgassing events consists of ^4He , ^{36}Ar and ^{40}Ar (see §I), so we assume a mean molar mass for the model gas of $\mu \approx 20$ g mol $^{-1}$, hence 940 kg of gas necessary to create an explosive outgassing event. The temperature at this depth is $\sim 0^\circ\text{C}$ (see §4), consequently implying an overall volume of gas of 2400 m 3 or a sphere 8.3 m in radius. What flow rate is needed to support this?

Using Fick’s diffusion law, $j = -K \, dn/dz$, where the gas number density $n = 1.1 \times 10^{19}$ cm $^{-3}$ is taken from above, dropping to zero through 15 m of regolith in z . The diffusivity K is 7.7 and 2.3 cm 2 s $^{-1}$ for He and Ar, respectively, in the Knudsen flow regime for basaltic lunar soil simulants (Martin et al. 1973¹), so we adopt $K = 5$ cm 2 s $^{-1}$ for our assumed He/Ar mixture. (For any other gas mixture of this molecular weight, K would likely be smaller; below we also show that K tends to be lower for real regolith.) Over the area of the gas reservoir, this implies a mass leakage rate of 2.8 g s $^{-1}$, or $\sim 40\%$ of the total SIDE rate. With the particular approximations made about the regolith diffusivity, this is probably near the upper limit on the leakage rate. At the surface of the regolith, this flow is spread to a particle flux of only $\sim 10^{16}$ cm $^{-2}$, which presumably causes no directly observable optical effects. The characteristic time to drain (or presumably fill) the reservoir is 4 d.

We consider the outgassing event occurring in two parts. Initially, the gas bubble explodes upward propelling regolith with it until it reaches the level of the surface; we assume that the plug contains a cone within 45° of the axis passing from the gas reservoir to the surface, normal to the surface. Through this process the gas and regolith become mixed. At this point, the gas expands from radius $r \approx 15$ m and drags the regolith outward until the dust cloud reaches a sufficiently small density to allow the gas to escape freely into the vacuum and the regolith to fall eventually to the surface. We consider this to be the “minimal TLP” for explosive outgassing, as there is no additional reservoir that is liberated by the event, beyond the minimum to puncture the regolith. One could also imagine triggering the

¹For the relatively nonreactive gases He and Ar, the diffusivity is proportional to $(T/\mu)^{1/2}$, where T is the absolute temperature. The sticking time of the gas molecules, or heat of absorption, becomes significant if the gas is more reactive or the temperature is reduced. Unfortunately we find no such numbers for real regolith, although we discuss realistic diffusivities for other gases below.

event by other means, many of which might release larger amounts of gas other than that poised at hydrodynamical instability. Undoubtably the release mechanism is more complex than that adopted here, but this release mode is sufficiently simple to be modeled.

We model this with a detailed (but not 3-D) code dealing with the evolution of dust shells (and often entrained gas) centered on the explosion point. Salient elements of the model include: 1) The regolith is binned into several divisions of different mean particle size (608 logarithmically spaced bins). Each bin is assumed to contain particles initially mixed evenly through the gas; 2) To represent the volume of regolith entrained in the gas, we create a series of 1000 concentric hemispherical shells for each of the 608 different particle size bins. Each of these shells for each particle size is now independent of each other and totally dependent on the gas-pressure and gravity for motion; 3) We further assume that each regolith shell remains hemispherical. Explicitly, we trace the dynamics of each shell with a point particle, initially 45 degrees from the base of the shell; 4) We calculate the outward pressure of the gas exerted on the dust. The force from this pressure is distributed among different shells of regolith particle size weighted by the total surface area of the grains in each shell. We calculate each shell's acceleration and integrate the equations of motion for a timestep $dt = 0.001$ s. 5) We calculate the diffusivity of each radial shell (in terms of the ability of the gas to move through it) by dividing the total surface area of all dust grains in a shell by the surface area of the shell itself (assuming grains surfaces to be spherical); 6) Starting with the largest radius shell, we sum the opacities of each shell until we reach a gas diffusive opacity of unity; 7) Any gas outside of the unit opacity shell is assumed to escape and is dropped from the force expansion calculation. Dust shells outside the unit opacity radius are assumed to now be ballistic and are dropped from the gas-opacity calculation. 8) We monitor the trajectory of each dust shell (represented by its initially 45° particle) until it drops to an elevation angle of 30° (at which point most of the gas is expanding above the particle), at which time this particle shell is no longer supported by the gas, and is dropped from the gas-opacity calculation; 9) An optical opacity calculation is made to determine the ability of an observer to see the lunar surface when looking down on the cloud. We calculate the downward optical opacity (such as from Earth) by dividing the total surface area of the dust grains in a shell by the surface area of the shell as seen from above (πr^2). Starting with the outmost dust shell, we sum downward-view optical opacities until we reach optical depth $\tau = 1$ and $\tau = 0.1$ to keep track the evolution of this cloud's appearance as seen from a distance; 10) We return to step #4 above and iterate one more timestep dt , integrating again the equations of motion. We continue this until all gas is lost and all dust has fallen to the ground. 11) For this model, we adopt a regolith particle size distribution consistent with sample 72141,1 (from McKay et al. 1974), which is shown over a range from $d = 8\text{mm}$ to $2\mu\text{m}$. Other sources (Basu & Molinaroli 2001) indicate a component extending below $2\mu\text{m}$, thus we extend our size distribution linearly from $2\mu\text{m}$ to $0\mu\text{m}$. We assume the regolith

particles are spherical in shape and do not change in shape or size during the explosion.

Finally, when all dust has fallen out, we calculate where the regolith ejecta has been deposited. With a template function for the deposition of a ballistic explosion of a spherical shell of material, we apply this template to the final resting radius of each shell to approximate the total deposition of material from the shell. We then sum all of the material from the 608,000 shells to determine the overall dust ejecta deposition profile.

There are obvious caveats to this calculation. First, the diffusion constant, and therefore the minimal flow rate, might be overestimated due to the significant (but still largely unknown) decrease in regolith porosity with increasing depth on the scale of meters (Carrier et al. 1991), plus the likelihood that simulants used have larger particles and greater porosity than typical regolith. Secondly, the regolith depth of 15 meters might be an overestimate for some of these regions, which are among the volcanically youngest and/or freshest impacts on the lunar surface. This exception does not apply to Plato and its active highland vicinity, however, and Aristarchus is thickly covered with apparent pyroclastic deposits which likely have different but unknown depths and diffusion characteristics.

3.2. Results from Explosive Outgassing Model

We find results for this “minimal TLP” numerical model of explosive outgassing through the lunar regolith interesting in terms of the reported properties of TLPs. Figure 1 shows the evolution of the model explosion with time, as might be seen from an observer above, in terms of the optical depth $\tau = 1$ and $\tau = 0.1$ profiles of the model event, where $\tau = 1$ is a rough measure of order unity changes in the appearance of the surface features, whereas $\tau = 0.1$ is close to the threshold of the human eye for changes in contrast, which is how many TLPs are detected (especially the many without noticable color change). In both cases the cloud at the particular τ threshold value expands rapidly to a nearly fixed physical extent, and maintains this size until sufficient dust has fallen out so as to prevent any part of the cloud from obscuring the surface to this degree.

Easily-seen effects on features ($\tau = 1$) lasts for 25 s and extends over a radius of 2 km, corresponding to 2 arcsec in diameter, resolvable by a typical optical telescope but often only marginally so. In contrast, the marginally detectable $\tau = 0.1$ feature extends over 14 km diameter (7.5 arcsec), lasting for 90 s, but is easily resolved. This model “minimal TLP” is an interesting match to the reported behavior of non-instantaneous ($\lesssim 1$ s) TLPs: about 7% of duration 90 s or less, and half lasting under about 1300 s. Certainly there should be selection biases suppressing reports of shorter events. Most TLP reports land in an envelope between about two minutes and one hour duration, and this model event lands at the lower

edge of this envelope. Furthermore, most TLPs, particularly shorter ones, are marginally resolved spatially, as would be the easily-detectable component of the model event. This correspondence also seems interesting, given the simplicity of our model and the state of ignorance regarding relevant parameters.

How might this dust cloud actually affect the appearance of the lunar surface? First, the cloud should cast a shadow that will be even more observable than simple surface obscuration, blocking the solar flux from an area comparable to the $\tau = 1$ region and visible in many orientations. Experiments with agitation of lunar regolith (Garlick et al. 1972b) show that the reflectance of dust is nearly always increased under fluidization, typically by about 20% and often by about 50% depending on the orientation of the observer versus the light source versus the cloud. Similar results should be expected here for our regolith cloud. These increases in lunar surface brightness would be easily observable spread over the many square kilometers indicated by our model.

Furthermore, because the sub-micron particle sizes dominate the outer regions of the cloud, it seems reasonable to expect Mie-scattering effects in this region with both blue and red clouds expected from different Sun-Earth-Moon orientations. Figure 2 shows the typical fall-out time of dust particles as a function of size. Particles larger than about $30\ \mu\text{m}$ all fall out immediately (within the first few seconds), whereas after a few tens of seconds, particles are differentiated for radii capable of contributing to wavelength-dependent scattering. Later in the event we should expect significant color shifts (albeit not order-unity changes in flux ratios).

Particle segregation or elutriation of dust in a cloud agitated by a low-density gas, as occurs in this model, has other effects in particular the generation of large electrostatic voltages. This leads to its own observable effects; we continue this part of the discussion in Appendix I.

The larger dynamical effects in the explosion cloud change rapidly over the event. Half of the initially entrained gas is lost from the cloud in the first 3 s, and 99% is lost in the first 15 s. Throughout the observable event, the remaining gas stays in good thermal contact with the dust, which acts as an isothermal reservoir. Gas escaping the outer portions of the dust cloud does so at nearly the sound speed ($\sim 420\ \text{m s}^{-1}$), and the outer shells of dust also contain particles accelerated to similar velocities. Gas escaping after about 3 s does so from the interior of the cloud in parcels of gas with velocities decreasing roughly inversely with time. One observable consequence of this is the expectation that much of the gas and significant dust will be launched to altitudes up to about 50 km, where it may be observed and might affect spacecraft in lunar orbit.

The longterm effects of the explosion are largely contained in the initial explosion crater

(nominally 14 m in radius), although exactly how the ejecta ultimately settle in the crater is not handled by the model. At larger radii the model is likely to be more reliable; Figure 3 shows how much dust ejecta is deposited by the explosion as a function of radius. Beyond the initial crater, the surface density of deposited material varies roughly as $\mu \propto r^{-2.6}$, so converges rapidly with distance. Inside a radius of ~ 1 km, the covering factor of ejecta is greater than unity; beyond this one expects coverage to be patchy. This assumes that the crater explosion produces few “rays.” The explosion can change the reflectivity by excavating fresh material, which would be evidenced due to a $\sim 10\%$ drop in reflectance at wavelength $\lambda \approx 950$ nm caused by surface Fe^{2+} states in pyroxene and similar minerals (Adams 1974, Charette et al. 1976). Likewise there is an increase in reflectivity in bluer optical bands (Buratti et al. 2000) over hundreds of nm. Even though these photometric effects are compositionally dependent, we are interested only in differential effects: gradients over small distances and rapid changes in time. The lifetime of even the effect at 1 km radius is short-lived, however, due to impact “gardening” turnover. The half-life of the ejecta layer at 1 km radius is only of order 1000 y (from Gault et al. 1974), and shorter at large radius (unless multiple explosions accumulate multiple layers of ejecta). At 30 m radius the half-life is of order 10^6 y. From maturation studies of the 950 nm feature (Lucey et al. 2000, 1998), even at 30 m, overturn predominates over optical maturation rates (hundreds of My timescales).

The scale of outgassing in this model event, both in terms of gas release ($\gtrsim 1$ tonne) and timescale ($\gtrsim 4$ d), are consistent with the total gas output and temporal granularity of outgassing seen in ^{40}Ar , a dominant lunar atmospheric component. The fact that this model also recovers the scale of many features actually reported for TLPs lends credence to the idea that outgassing and TLPs might be related to each other causally in this way, as well as circumstantially via the Rn^{222} episodes and TLP geographical correlation described in Paper I.

How often such an event due to outgassing puncturing the regolith layer should occur is unknown, due to the uncertainty in the magnitude and distribution of endogenous gas flow to the surface, and to some degree how the regolith reacts in detail to large gas flows propagating to the surface. Also, a new crater caused by explosive outgassing will change the regolith depth, its temperature structure, and eventually its diffusivity. We will not attempt here to follow the next steps in the evolution of an outgassing “fumerole” in this way, but are inspired to understand how regolith, its temperature profile, and gas interact, as in the next section. Furthermore, such outgassing might happen on much larger scales, or might over time affect a larger area. Indeed, such a hypothesis is offered for the scoured region of depleted regolith forming the Ina D feature and may extend to other regions around Imbrium (Schultz et al. 2006).

Our results here and in Paper I bear directly on the argument of Vondrak (1977) that TLPs as outgassing events are inconsistent with SIDE episodic outgassing results. The detection limits from ALSEP sites *Apollo 12*, *14* and *15* correspond to 16-71 tonne of gas per event at common TLP sites, particularly Aristarchus. (Vondrak states that given the uncertainties in gas transportation, these levels are uncertain at the level of an order of magnitude.) Our “minimal TLP event” described above is 20-80 times less massive than this, however, and still visible from Earth. It seems implausible that a spectrum of such events would never exceed the SIDE limit, but it is not so obvious such a large event would occur in the seven-year ALSEP operations interval. Also, this SIDE limit interpretation rests crucially on the existence of Alphonsus (and Ross D) as prime TLP sites, both features which are rejected by our robust geographical TLP sieve in Paper I.

4. Seepage of Gas Through the Regolith

Referring back to scenarios (2) and (3) in §2, the onset of fluidization (Mills 1969) marks the division between these two regimes of seepage and “bubbling” and has been studied (Siegal & Gold 1973, Schumm 1970). Although laboratory tests are made with coarser sieve particulates and much thinner dust layers in 1 *g* gravity, we can scale the gas pressure needed for incipient fluidization by g^{-2} and thickness t^1 to find the threshold $P = 0.16$ atm (Siegal & Gold 1973). Correcting for less diffusive regolith, this pressure estimate is likely a lower limit. Below this pressure simple gas percolation likely predominates.

What processes occur during “simple” percolation? Were it not for phase changes of venting gas within the regolith, the composition of the gas might be a weak consideration in this paper (except for perhaps the molecular/atomic mass), and temperature would likely only affect seepage as $T^{1/2}$ in the diffusivity. Water plays a special role in this study (separate from concerns regarding resource exploitation or astrobiology), in that it is the only common substance encountering its triple point temperature in passing through the regolith, at least in many locations. In this case water might not contribute to overpressure underneath the regolith which might lead to explosive outgassing. This would also imply that even relatively small volatile flows containing water might tend to freeze in place and remain until after the flow stops. For water this occurs at 0.01°C, corresponding to 0.006 atm in pressure (the pressure dropping by a factor of 10 every $\sim 25^\circ$.)

Effectively, water is the only relevant substance to behave in this fashion. The next most common substances may be large hydrocarbons such as nonane or benzene, obviously not likely abundant endogenous effluents from the interior. Also H_2SO_4 reaches its triple point, but changes radically with even modest concentrations of water. A similar statement can be

made about HNO_3 , not a likely outgassing constituent. These will not behave as their pure state, either; this leaves only H_2O . Water (and sulfur), on the other hand, has been found in significant concentration in volcanic glasses from the deep lunar interior (Saal et al. 2008, Hauri et al. 2009), and has been liberated in large quantities in past volcanic eruptions. The measured quantities of tens of ppm imply juvenile concentrations of hundreds of ppm.

From the heat flow measurements at the *Apollo 15* and *17* lunar surface experiment (ALSEP) sites (Langseth & Keihm 1977), we know that just below the surface, the stable regolith temperature is in the range of 247-253K (dependent on latitude, of course), with gradients (below 1-2 m) of 1.2-1.8 deg m^{-1} , which extrapolates to 0°C at 13 – 16 m depths subsurface. With the exception of the outermost few centimeters, the entire regolith is below the triple point temperature and is too deep to be affected significantly by variations in heating over monthly timescales. This is an interesting depth, since in many areas the regolith is not quite this deep, as small as under a few meters near Lichtenberg (Schultz & Spudis 1983) and at the Surveyor 1 site near Flamsteed (Shoemaker & Morris 1970) to depths at Apollo sites (summarized by McKay et al. 1991) near the 0°C depths calculated above, up to probably 20 m or more in the highlands, and 40 m deep north of the South Pole-Aitken Basin (Bart & Melosh 2005). Presumably, the fractured megaregolith supporting the regolith likely does not contain as many small particles useful for retaining water ice, as we detail below, but may also accumulate ice temporarily. A more recent heat flow analysis (Saito et al. 2007) accounting for longer timescale fluctuations would place the 0°C depth at least twice as far under the surface, increasing the lifetime of retained volatiles against sublimation accordingly, but for now we shall proceed with a more conventional, shorter-lived analysis.

The escape of water and other volatiles into the vacuum is regulated by the state of the regolith and is presumably largely diffusive. For this discussion we assume the Knudsen flow regime (low-density, non-collisional gas) is relevant. Of special importance is the measured abundance of small particle sizes evident in the upper levels of the regolith, which perhaps pertains to depths ~ 15 m (where bulk density is probably higher: Carrier et al. 1991). Assuming that particle distributions are self-similar in size distribution (constant porosity), for random-walk diffusion out of a volume element dV , the diffusion time step presumably scales with the particle size a , so the diffusion time t as a^{-1} . For particles of the same density, therefore, one should compute the diffusion time by taking a a^{-1} -weighted average of particle sizes counted by mass. $\langle a \rangle$. This moment of the distribution is the same relevant in the previous section.

Published size distributions measured to sufficiently small sizes include again McKay et al. (1974) with $\langle a \rangle = 24 \mu\text{m}$, and supplemented on smaller sizes with *Apollo 11* sample 10018 (Basu & Molinaroli 2001), which reduces the average to about $20 \mu\text{m}$. This is an

overestimate because a large fraction (34-63%) are agglutinates, which are groupings of much smaller particles, many agglutinates with effective areas e.g., $e = A/4\pi r^2$, with values of a few up to 8. (Here r is a mean radius from the center of mass to a surface element.) To a gas particle, the sub-particle size is more relevant than the agglutinate size, so the effective particle size of the entire sample might be considerably smaller, conceivably by a factor of a few.

We compare this to experimental simulations, a reasonably close analogy being the sublimation of a water of ice buried up to 0.2 m below a medium of simulant JSC Mars-1 (Allen et al. 1998) operating at $\sim 263^\circ\text{K}$ and 7 mbar (Chevrier et al. 2007), close to lunar regolith conditions. This corresponds to the lifetime of 800 y for a 1 m ice layer below the surface by 1 m. The porosity of JSC Mars-1 is 44-54%, depending on compactification, versus for lunar soil about 49% at the surface and perhaps 40% at a depth of 60 cm and slightly lower at large depths (Carrier et al. 1991). Lunar soil is slightly less diffusive by solely this measure. The mean size $\langle a \rangle$ of JSC Mars-1 is 93 μm , $\gtrsim 10$ times larger than that for *Apollo 17* and *11* regolith, accounting for agglutinates, so the corresponding timescale for regolith material is, very approximately, $\gtrsim 10$ ky (perhaps up to ~ 30 ky). Other simulants are more analogous to lunar regolith, so that such experiments in the future might be made more closely relevant.

Converting a loss rate for 1 m below the surface to 15 m would involve the depth ratio R . Farmer (1976) predicts an evaporation rate scaling as R^{-1} (as opposed to the no-overburden analysis: Ingersoll 1970). Experiments with varying depths of simulated regolith (Chevrier et al. 2007) show that the variation in lifetime indeed goes roughly as R^1 , implying a 1 m ice slab lifetime at 15 m on the order of 10^5 to 3×10^5 y. The vapor pressure for water ice drops a factor of 10 in passing from 0°C to current temperatures of about -23°C just below the surface (also the naked-ice sublimation rate: Andreas 2007), which would indicate that $\sim 90\%$ of water vapor tends to stick in overlying layers (without affecting the lifetime of the original layer, coincidentally). This begs the question of the preferred depth for an ice layer to form. The regolith porosity decreases significantly between zero and 1 m depth (Carrier et al. 1991) which argues weakly for preferred formation at greater depth. At 30 m depth or more, the force of overburden tends to close off porosity.

The current best limit on water abundance is from the sunrise terminator abundances from LACE, which produces a number ratio of $\text{H}_2\text{O}/^{40}\text{Ar}$ with a central value of 0.014 (with 2σ limits of 0-0.04), which might indicate an actual $\text{H}_2\text{O}/^{40}\text{Ar}$ outgassing rate ratio up to 5 times higher (Hoffman & Hodges 1975). Adopting the SIDE rate of 7 g s^{-1} in the ~ 20 -44 AMU mass range, and assuming most of these are ^{40}Ar (Vondrak, Freeman & Lindeman 1974: given the much lower solar wind contributions of other species in this range), this translates to 0.1 g s^{-1} in water (perhaps up to 0.5 g s^{-1} or 15 tonne y^{-1}), in which case most

of the gas must be ionized). The disagreement between SIDE and LACE is a major source of uncertainty (perhaps due to the neutral/ionized component ambiguity).

We discuss below that at earlier times the subsurface temperature was likely lower, but let us consider now the situation in which a source arises into pre-established regolith in recent times. We assume a planar diffusion geometry, again. In this case, take spatial gradients over 15 m, and scale the JSC Mars-1 diffusivity of $1.7 \text{ cm}^2 \text{ s}^{-1}$ to $0.17 \text{ cm}^2 \text{ s}^{-1}$ for lunar regolith. Since the triple-point pressure corresponds to number density $n = 2.4 \times 10^{17} \text{ cm}^{-3}$, the areal particle flux density is $j = 2.7 \times 10^{13} \text{ s}^{-1} \text{ cm}^{-2}$. For a large outgassing site, with the same water fraction of water indicated by LACE e.g., total outgassing of 7 g s^{-1} including 0.1 g s^{-1} of water, this rate can maintain a total area of 0.012 km^2 at the triple-point pressure i.e., a 125 m diameter patch. This is much larger than the 15 m regolith depth, bearing out our assumed geometry. If this ice patch were 1 m thick, for example, the ice would need to be replenished every 4000 y.

Of course, this is a simple model and many complications could enter. We consider briefly, for instance, the effects of latitude, change in lunar surface temperature over geological time, and the effects of aqueous chemistry on the regolith.

4.1. Latitude Effects

The temperature just below the surface is legislated by the time-averaged energy flux in sunlight, so scales according to the Stefan-Boltzmann law from the temperature at the equator ($\phi = 0$) according to $T(\phi) = T(0)\cos^{1/4}(\phi)$. This predicts a 6K temperature drop from the equator (at about 252K) to the latitude of the Aristarchus Plateau ($\phi \approx 26^\circ$) or the most polar subsurface temperature measurement by *Apollo 15*, a drop to 224K at Plato ($\phi = 51^\circ.6$), $\lesssim 200\text{K}$ for the coldest 10% of the lunar surface ($\phi > 65^\circ$) and $\lesssim 150\text{K}$ for the coldest 1% ($\phi > 82^\circ$).² These translates into a regolith depth corresponding to the water triple-point about 4, 18, 33 or 65 m deeper than at the equator, respectively. Permanently shadowed cold traps, covering perhaps 0.1% of the surface, have temperatures $\lesssim 60\text{K}$ (e.g., Adorjan 1970, Hodges 1980). (Note that the lunar South Pole is a minor TLP site responsible for about 1% of robust report counts.) Since even at the equator the H_2O triple point temperature occurs about 13 m below the surface, at increasing latitude this zone quickly moves into the megaregolith of less pulverized material where the diffusivity is largely unknown but presumably higher (neglecting the decrease in porosity due to compression by

²The most polar maria edge might be considered that of Mare Frigoris at $\phi \approx 65^\circ$, but there are flooded craters much higher.

overburden). To study this, then, we assume a layer of regolith 15 m deep of low diffusivity material overlying a high diffusivity layer which may be populated by channels which can direct gas quickly upward (although perhaps not so easily horizontally).

The diffusivity of the regolith near 0°C is dominated by elastic reflection from mineral surfaces, without sticking, whereas at lower temperatures H₂O molecules stick during most collisions (Haynes, Tro & George 1992). This is especially the case if the surfaces are coated with at least a few molecular layers of H₂O molecules, of negligible mass. The sticking behavior of H₂O molecules on water ice has been studied over most of the temperature range relevant here (Washburn et al. 2003; but does depend somewhat on whether the ice is crystalline or amorphous: Speedy et al. 1996). In contrast the sticking behavior of H₂O molecules on lunar minerals is much less well known.

The lunar simulant diffusivity value above corresponds to a mean free path time of about 1 μ s for H₂O molecules near 0°C. In contrast the timescale for H₂O molecules sticking on an ice surface is (from Schorghofer & Taylor [2007] and references therein): $\tau = \theta / (\alpha P_v / \sqrt{2\pi k T \mu})$, where θ is the areal density of H₂O molecules on ice $\theta = (\rho/\mu)^{2/3} \approx 10^{15}$ cm⁻² for density ρ , molecular mass μ . The sticking fraction α varies from about 70% to 100% for $T = 40$ K to 120K. The equilibrium vapor pressure is given by $P_v = p_t \exp[-Q(\frac{1}{T} - \frac{1}{T_t})/k]$ where p_t and T_t are the triple point pressure and temperature, respectively, and sublimation enthalpy $Q = 51.058$ kJ/mole. This expression and laboratory measurements imply a sticking timescale $\tau \approx 1$ μ s at $T = 260$ K, 1 ms at 200K, 1 s at 165K, 1 hr at 134K, and 1 yr at 113K. The sticking timescale quickly and drastically overwhelms the kinetic timescale at lower temperatures, and ice patches can last for geological timescales.

This molecular behavior has a drastic effect on the size of the ice patch maintained by the example source considered above. Simply scaling by the time between molecular collisions, corresponding to a 125 m diameter ice patch at $\phi = 0$, we find at the base of the regolith a 160 m patch at $\phi = 26^\circ$ (Aristarchus Plateau), 580 m at $\phi = 51^\circ.6$ (Plato), 2.3 km at $\phi = 65^\circ$ (10% polar cap), and an essentially divergent value, 522 km at $\phi = 82^\circ$ (1% polar cap). If in fact the regolith layer is much deeper than suspected, the added depth of low diffusivity dust significantly increases the patch area: 170 m at $\phi = 26^\circ$, 830 m at $\phi = 51^\circ.6$, and 4 km at $\phi = 65^\circ$.

4.2. Longterm Evolution

Most portions of the lunar surface have been largely geologically inactive during the past 3 Gy or more (with some of the notable exceptions listed above). During this time several important modifications of the scenario above are relevant.

The current heat flow from the lunar interior, $j_{int} \approx 0.03 \text{ W m}^{-2}$ (Langseth et al. 1972, 1973), is only 2×10^{-5} of the solar constant, so affects the surface temperature only ~ 1.3 millidegree. There were times in the past, however, when interior heating presumably pushed the temperature near the surface over 0°C . Nonetheless, ice that formed Gy ago might still survive from when outgassing was nearly purely volcanic, not radiogenic.

To even consider the zero-degree zone near the maria, this presumably requires waiting until ~ 3 Gy b.p., probably sufficient for the Moon globally (see Spohn et al. 2001). After this point the 0°C depth will recede into the regolith, while the regolith layer is also growing. On the other hand, at this time the average surface temperature was cooler by ~ 15 degree due to standard solar evolution (Gough 1981 – perhaps 17° lower in the highlands at 4 Gy b.p.). Since the thickness of regolith after 3 Gy b.p. grows at only about 1 m per Gy (Quaide & Oberbeck 1975), within the maria the 0°C depth sinks into bedrock/fractured zone. Whatever interaction and modification might be involved between the regolith and volatiles will proceed inwards, leaving previous epochs’ effects between the surface vacuum and the 0°C layer now at ~ 15 m.

4.3. Chemical Interactions with Regolith

Another issue is possible regolithic chemical reactions with outgassing volatiles, especially over prolonged geological timescales. The key issue is the possible presence of water vapor, and perhaps SO_2 . There is little experimental work on the aqueous chemistry of lunar regolith (which will vary due to spatial inhomogeneity). Dissolution of lunar fines by water vapor is greatly accelerated in the absence of other gases such as O_2 and N_2 (Gammage & Holmes 1975), and appears to proceed by etching the numerous damage tracks from solar-wind particles. This process acts in a way to spread material from existing grains without reducing their size (which would otherwise tend to increase porosity). Liquid water is more effective than vapor, not surprisingly, and ice tends to establish a pseudo-liquid layer on its surface. This is separate from any discussion of water retention on hydrated minerals surfaces robust to temperatures above 500°C (Cocks et al. 2002 & op cit.).

This is a complex chemical system that will probably not be understood without simulation experiments. The major constituents are presumably silicates, which will migrate in solution only over geologic time. (On Earth, consider relative timescales of order 30 My typical migration times for quartz, 700 ky for orthoclase feldspar, KAlSi_3O_8 and 80 ky for anorthite, $\text{CaAl}_2\text{Si}_2\text{O}_8$: Brantley 2004.) One might also expect the production of $\text{Ca}(\text{OH})_2$, plus perhaps $\text{Mg}(\text{OH})_2$ and $\text{Fe}(\text{OH})_2$. It is not clear that $\text{Fe}(\text{OH})_2$ would oxidize to more insoluble $\text{FeO}(\text{OH})$, but any free electrons would tend to encourage this. It seems that the

result would be generally alkaline. Since feldspar appears to be a major component in some outgassing regions e.g., Aristarchus (McEwen et al. 1994), one should also anticipate the production of clays. This is not accounting for water reactions with other volatiles e.g., ammonia, which has been observed as a trace gas (Hoffman & Hodges 1975) perhaps in part endogenous to the Moon, and which near 0°C can dissolve in water at nearly unit mass ratio (also to make an alkaline solution). Carbon dioxide is a possible volatile constituent, and along with water can metamorphose olivine/pyroxene into $\text{Mg}_3\text{Si}_4\text{O}_{10}(\text{OH})_2$ i.e. talc, albeit slowly under these conditions; in general the presence of CO_2 and thereby H_2CO_3 opens a wide range of possible reactions into carbonates. Likewise the presence of sulfur (or SO_2) opens many possibilities e.g., $\text{CaSO}_4 \cdot 2\text{H}_2\text{O}$ (gypsum), etc. Since we do not know the composition of outgassing volatiles in detail, we will probably need to inform simulation experiments with further remote sensing or in situ measurements.

The mechanical properties of this processed regolith are also difficult to predict. Some substances simple to produce are of very low hardness and not of high ductility. Some of these products expand but will likely fill the interstitial volume with material, which will raise its density and make it more homogeneous. Regolith is already ideal in having a nearly power-law particle distribution with many small particles. It seems likely that any such void-filling will sharply reduce diffusivity. The volatiles actually discovered in volcanic glasses from the deep interior (Saal et al. 2008, Hauri et al. 2009) include primarily H_2O and SO_2 but not CO_2 . With the addition of water, regolithic mineral combinations tend to be cement-like, and experiments with anorthositic lunar chemical simulants have produced high quality cement without addition of other substances, except SiO_2 (Horiguchi et al. 1996, 1998). Whether this happens *in situ* depends upon whether over geological time $(\text{CaO})_3\text{SiO}_2$ or other Ca can act as a binder without heating to sintering temperatures. The possible production of gypsum due to the high concentrations of sulfur would add to this cement-like quality. The extent to which ordinary mixes such as portland cement lose water into the vacuum depend on their content of expansive admixture (Kanamori 1995) Portland cement mixes show little evidence of loss of compressional strength in a vacuum (Cullingford & Keller 1992).

We need to think in terms of possibly cemented slabs in some vicinities, and need to consider the effects of cracks or impacts into this concrete medium. This is probably not a dominant process, since the overturn timescale to depths even as shallow as 1 m is more than 1 Gy (Gault et al. 1974, Quaide & Oberbeck 1975), whereas we discuss processes at ~ 15 m or more. Craters 75 m in diameter will permanently excavate to a 15 m depth (e.g., Collins 2001, and ignoring the effects of fractures and breccia formation), and are formed at a rate of about $1 \text{ Gy}^{-1} \text{ km}^{-2}$ (extending Neukum et al. [2001] with a Shoemaker number/size power-law index 2.9). This will affect some of the areal scales discussed above, but not all. We speculate that vapor or solution flow might tend to deliver ice and/or solute to these

areas and eventually act to isolate the system from the vacuum. Finally, we note above that over geological timescales this ice layer will tend to sink slowly into the regolith, at a rate of order 1 m Gy^{-1} , setting up a situation where any relatively impermeable concrete zone will tend to isolate volatiles from the vacuum. In this case volatile leakage will tend to be reduced to a peripheral region around the ice patch. Assuming that volatiles leak out through the entire 15 m thickness of regolith at the patch boundary, the 125 m diameter patch area for $\phi \approx 0$ from above corresponds to a peripheral zone expected from a 520 m diameter patch. Thus any such concrete overburden will encourage growth of small patches, and will do so even more for larger ones (assuming $\lesssim 15 \text{ m}$ regolith depth).

How much water might reasonably be expected to outgas at these sites? The earliest analyses of Apollo samples argued for extreme scarcity of water and other volatiles (Anders 1970, Charles, Hewitt & Wones 1971, Epstein & Taylor 1972). On the Earth, water is the predominant juvenile outgassing component (Gerlach & Graeber 1985, Rubey 1964), whereas even the highest water concentrations discussed below (Saal et al. 2008) imply values an order of magnitude smaller. On the Moon, water content is drastically smaller, with a current atmospheric water content much less than what would affect hydration in lunar minerals (Mukherjee & Siscoe 1973), although some lunar minerals seem to involve water in their formation environments (Agrell et al. 1972, Williams & Gibson 1972, Gibson & Moore 1973, and perhaps Akhmanova et al. 1978). The origin of the water in volcanic glasses (Saal et al. 2008, Hauri et al. 2009) is still poorly understood but implies internal concentrations that at first look seems in contradiction with earlier limits e.g., Anders 1970. For much different lunar minerals, high concentration is implied for water (McCubbin et al. 2007) as well as other volatiles (Krähenbühl et al. 1973).

It is not a goal of this paper to explain detected water in lunar samples, but its origin at great depth is salient here. As a point of reference, Hodges and Hoffman (1975) show that the ^{40}Ar in the lunar atmosphere derives from deep in the interior, of order 100 km or more. They hypothesize that the gas could just as easily derive from the asthenosphere, 1000 km deep or more (see also Hodges 1977). The picritic glasses analyzed by Saal, Hauri, et al. derive from depths of $\sim 300\text{-}400 \text{ km}$ or greater (Elkins-Tanton et al. 2003, Shearer, Layne & Papike 1994). O_2 fugacity measurements e.g., Sato 1979, are based on glasses from equal or lesser depths. Water originating from below the magma ocean might provide one explanation (Saal et al. 2008), as might inhomogeneity over the lunar surface. Differentiation might not have cleared volatiles from the deep interior despite its depletion partially into the mantle. One might also consider that geographical variation between terranes e.g., KREEP or not, might be important.

While the temperature of the proto-Earth and progenitor impactor material in simulations grow to thousands of Kelvins, sufficient to drive off the great majority of all volatiles,

these are not necessarily the only masses in the system. Either body might be orbited by satellites containing appreciable volatiles, which would likely not be heated to a great degree and which would have a significant probability of being incorporated into the final moon. Furthermore, there is recent discussion of significant water being delivered to Earth/Moon distances from the Sun in the minerals themselves (Lunine et al. 2007, Drake & Stimpfl 2007), and these remaining mineral-bound even at high temperatures up to 1000K (Stimpfl et al. 2007). The volume of surface water on Earth is at least $1.4 \times 10^9 \text{ km}^3$, so even if the specific abundance of lunar water is depleted to 10^{-6} terrestrial, one should still expect over 10^{10} tonnes endogenous to the Moon, and it is unclear that later differentiation would eliminate this. This residual quantity of water would be more than sufficient to concern us with the regolith seepage processes outlined above.

For carbon compounds, models of the gas filling basaltic vesicles (Sato 1976; see also O’Hara 2000, Wilson & Head 2003, Taylor 1975) predict CO, COS, and perhaps CO₂ as major components. In fact negligible CO₂ is found in fire-fountain glasses originating from the deep interior (Saal et al. 2008); this should be considered in light of CO on the Moon (and CO₂ on Earth) forming the likely predominant gas driving the eruption (Rutherford & Papale 2009).

We suspect that water outgassing was likely higher in the past than it is now. Furthermore, no site of activity traced by ²²²Rn or by robust TLP counts (Paper I) has been sampled. (The sample return closest to Aristarchus, *Apollo 12*, is 1100 km away.)³ From our discussion above the behavior of outgassing sites near the poles versus near the equator might differ greatly, with volatile retention near the poles being long-term and perhaps making the processing of volatiles much more subterranean and covert. (Note that the lunar South Pole is a minor TLP site responsible for about 1% of robust report counts, as per Paper I.)

With these uncertainties we feel unable to predict exactly how or where particular evidence of lunar surface outgassing might be found, although the results from above offer specific and varied signals that might be targetted at the lunar surface. For this reason we turn attention to how such effects might be detected realistically from the Earth, lunar orbit, and near the Moon’s surface, and suggest strategies not only for how might be tested but also how targetted observations might economically provide vital information about the nature of lunar outgassing.

³The only persistent TLP site of some statistical significance that corresponds to a sample return (170 g from Luna 24) is Mare Crisium, ambiguous in several ways: 1) the robust TLP report count for Crisium is only zero to 6, depending on the robustness filter employed (Paper I); 2) the nature of this robust count is problematic given the extended nature of Crisium as a feature, and 3) the sample returned from Crisium is one case where the absence of water in the sample is ambiguous (Akhmanova et al. 1978).

We appreciate the controversial nature of suggesting small but significant patches of sub-surface water ice, given the history of the topic. We take care to avoid “cargo cult science” - selection of data and interpretation to produce dramatic but subjectively biased conclusions that do not withstand further objective scrutiny (Feynman 1974). Despite the advances made primarily by Apollo-era research, we are still skirting the frontiers of ignorance. We are operating in many cases in a regime where interesting observations have been made but the parameters e.g., the endogenous lunar molecular production (water vapor or otherwise), required to evaluate alternative models and interpretations are sufficiently uncertain to frustrate immediate progress. Below we offer several straightforward and prompt tests of our conclusions and hypotheses which offer prospects of settling many of these issues.

5. Observational and Experimental Techniques

TLPs are infrequent and short-lived, an overwhelming fact to be surmounted in their study. We envision nested observational methods to overcome this circumstance, with its currently anecdotal and bias-ridden data set, replacing it with a new data set with *a priori* explicit, calculable selection effects. This might seem daunting, since in Paper I we used essentially all known reports from visual lunar observations since the invention of the telescope! With modern imaging and computer techniques, this is tractable.

Another problem clear above is the variety of ways in which outgassing can interact with the regolith. In cases of slow seepage, gases may long delay their escape from the regolith. If the gases are volcanic, they might interact along the way, and water vapor is might trap it and other gases in the regolith. These factors bear on designing future investigations.

We can make significant headway. Difficulties due to paucity of TLP data leave avenues that modern technology can exploit. Table 1 lists the many methods detailed in this section. There has been no areal-encompassing, digital image monitoring of the Near Side with appreciable time coverage using modern software techniques to isolate transients. There are no published panspectral maps at high spectral/spatial resolution of the Near Side, beyond that usually called multispectral imaging. (To some degree this might be remedied by the Moon Mineralogy Mapper, M³: Pieters et al. 2006 - onboard *Chandrayaan-1*, but this mission’s success is in doubt.) Numerous particle detection methods are promising. The relevant experiments on Apollo were limited in duration, a week or less, or 5-8 years in the case of ALSEP. Furthermore *Clementine* and the relevant portion of the *Lunar Prospector* missions were also relatively short. All of these limitations serve as background to the following discussions.

6. Discussion and Conclusions

The origin of transient lunar phenomena has been mysterious, and their correlation to outgassing, while strong, was only circumstantial. The plausible generation of TLP-like events via a straightforward consequence of outgassing from the lunar interior lends credence to the idea that we may have found a causal link. The model we have presented is necessarily tied to outgassing from deep below the regolith, in that we require that the gas be concentrated in a nearly point-like source via some deep crack or channel. A similar calculation for radiogenic gas evolved from the regolith is incapable of providing the concentration in pressure needed to produce a noticeable explosive event.

Apollo-era and later data were insufficiently sensitive to establish the level of outgassing beyond ^{222}Rn , ^{20}Ne and isotopes of Ar, plus He, presumably, and did detect marginally molecular gas, but of uncertain origin, particularly CH_4 . Reviewing the evidence and available techniques, there are several gases that should be highlighted as crucial outgassing tracers. ^{222}Rn (and its products e.g., ^{210}Po) can be detected remotely of course and are unique in terms of their mapping potential, while being a minor fraction of escaping gas, presumably. ^{40}Ar is a major mass constituent of the atmosphere and unlike ^4He is not confused with the solar wind. Both ^{222}Rn and ^{40}Ar will tend to favor KREEP terrane in the western maria, presumably.

If outgassing is coming from the deep interior, one cannot neglect the indication that at one time such gas was dominated by volcanic, molecular gas. Particular among these is water vapor, which passes through its triple point temperature in rising from the base to the surface of the regolith. Given a high enough concentration, therefore, one should expect the production of water ice. The conditions under the regolith, particularly near the lunar poles, are favorable for such ice to persist even over geological time interval. It is possible that ice generated there when outgassing was more active still remains. We further point out that the plausible chemical interaction of such molecular gases with the regolith is the production of cement-like compounds that might radically alter the diffusivity of the regolith. Given the temperature evolution of the regolith, this non-diffusive layer would isolate the volatile outflow from the vacuum.

The question remains how we will detect such molecular outgassing effects, given their largely covert nature; this is greatly complicated by possible anthropogenic contamination in the future. Among molecular gases, sulfur e.g., SO_2 is the predominate volatile detected in deep-interior fire fountain glasses, a key factor in deciding what to pursue as a volcanic tracer. Furthermore, essential no liquid or hybrid rocket propellant candidate contain sulfur, and the only sulfuric solid propellants are fairly outdated e.g., black powder and Zn-S. NASA and hopefully other space agencies have no plans to use these on lunar missions.

Despite the hypotheses and methods outlined above, there is great doubt regarding the nature of lunar outgassing. Water is of obvious and diverse interest, and CO_2 and CO , while missing as apparent constituents, are interesting as drivers for fire fountain eruption. Plausibly the only way to study these components reliably is before the new introduction of large spacecraft into the lunar environment. Given uncertainty of how these gases and SO_2 might interact with the regolith, this early study appears paramount.

The salient facts from the above treatment is that for many years yet monitoring for optical transients will still be best done from the Earth’s surface, even considering the important contributions that will be made by lunar spacecraft probes in the next several years. These spacecraft will be very useful in evaluating the nature of transient events in synergy with ground-based monitoring, however. Given the likely behavior of outgassing events, it is unclear that in-situ efforts alone will necessarily isolate their sources within significant winnowing of the field by remote sensing. Early placement of capable mass spectrometers of the lunar surface, however, might prove very useful in refining our knowledge of outgassing composition, in particular a dominant component that could be used as a tracer to monitor outgassing activity with more simple detectors. This should take place before significant pollution by large spacecraft, which will produce many candidate tracer gasses in their exhaust.

We do not know enough now to discuss the potential implications of this line of research in terms of resources for human exploration, or even in terms of prebiologic chemistry on the Moon and for tenuous endogenous outgassing and atmospheric interactions with the regolith on other bodies, but all of these are interesting, novel avenues of such research. It is crucial that exploration of these issues progress while we have a pristine lunar surface as our laboratory.

Acknowledgements

We would much like to thank Alan Binder and James Applegate, as well as Daniel Savin, Daniel Austin and the other members of AEOLUS (“Atmosphere as seen from Earth, Orbit and LUnar Orbit”) for helpful discussion. This research was supported in part by NASA (07-PAST07-0028 and 07-LASER07-0005), the National Geographic Society (CRE Grant 8304-07), and Columbia University.

Appendix I: Coronal Discharge Luminescence Caused by Outgassing

In §3 we see that dust particles may remain suspended for long times in a gas of number density 10^{10} to 10^{15} cm^{-3} on scales of several tenths to several km, a plausible venue for generating large electrostatic potentials (e.g., “volcano lightning”). Regolith consists of several predominant minerals in various particle size ranges; under suspension and acceleration by gas flow, dust particle charge segregation is possible.

For the following calculation we adopt a typical particle size of $r = 10$ μm , and a typical difference in work function $\Delta W = 0.5$ eV. The actual value ΔW for particles of even well-defined compositions is problematic due to surface effects such as solar-wind/micrometeoritic weathering and exposed surface Fe^{2+} states. The following analysis suffices for two particles of different conducting composition; a similar result arises via triboelectric interaction of two different dielectrics although the details are less understood. Disturbed dust is readily charged for long periods in the lunar surface environment (Stubbs, Vondrak & Farell 2005).

Two particles will exchange charge upon contact until the equivalent of $\pm 0.25\text{V}$ is maintained, amounting to $Q = CV = 4\pi\epsilon_0 rV = 2.8 \times 10^{-16}$ coul = 1700 e^- . When these two particles separate to a distance $d \gg r$, their mutual capacitance becomes $C_2 = 4\pi\epsilon_0 r^2/d$. For $d = 100$ m, assuming the particles retain Q , the voltage increases by 7 orders of magnitude! - which cannot be maintained.

Paschen’s curve for coronal discharge goes through a minimum potential at 137V for argon, 156V for helium, at column densities N of 3.2×10^{16} cm^{-2} and 1.4×10^{17} cm^{-2} , respectively. In carefully controlled conditions, breakdown in He at potentials as low as 20V can be achieved (Compton, Lilly & Olmstead 1920). Nominally, Paschen’s curves usually rise steeply for lesser column densities, and roughly proportional to N for larger column densities. The minimal-discharge column densities for molecules are similar to those for Ar and He, and minimum voltages several time higher e.g., 420V at 1.8×10^{16} cm^{-2} for CO_2 ; $\sim 430\text{V}$ for NH_3 , 414V for H_2S , and 410V for CH_4 , and similar N values for molecules e.g., 2.1×10^{16} cm^{-2} . These results are somewhat dependent of the structure and composition of the electrodes used in these measurements.

The visual appearance of atomic emission of these gasses in high voltage discharge tubes is well know, with He emitting a pink-orange glow (primarily from transitions at 4471.5Å, and 5875.7Å, plus 7065.2Å marginally visible to the naked eye: Reader & Corliss 1980, Pearse & Gaydon 1963), and Ar a violet glow (from many lines 4159Å to 4880Å). Ne, producing intense red emission (with many lines 5852Å to 7032Å) comes to mind, but is apparently not an endogenous gas. It is plausible that TLP emission achieving coronal discharge would produce similar output spectra; the incidence of intense red emission in some TLP reports (Cameron 1978) argues for some other gas. The most common candidate molecules produce coronal

emission that appears white or violet-white (CO_2 , SO_2) or red (water vapor - primarily $\text{H}\alpha$, which is produced in many hydrogen compounds; CH_4 - Balmer lines plus CH bands at 390 and 431 nm).

In comparison, the events and their colors actually reported can be counted (although there is a significant range in outcomes depending on how one categorizes mixed colors and other factors). Following Paper I, we divide the sample at year 1956 (the latter composing 1/4 of the sample); before 1956: red - 11, blue (or blue-green) - 7, violet - 5, yellow - 4, red-yellow - 3, brown - 2, orange - 2; after 1955: red - 52, violet - 3, orange - 1. In the later reports, three red events also contain elements of violet/blue, plus one with orange, plus one with blue. Evidently red reports are common (out of the total sample of 894, not including the reports by Bartlett, which are largely blue), however, there is a statistically significant change after 1956, where about 1/5 of reports include red color, many associated with Aristarchus. This change is presumably due to a shift in the nature of observers rather than the physics of lunar events.

The initial gas density at the surface from a minimal TLP is of the order 10^{18} cm^{-3} , meaning that the optimal column for coronal discharge might conceivably be achieved on centimeter scales, whereas the initial outburst is over tens of meters. By the time a minimal TLP has expanded to 1 km radius, the density has dropped to $\sim 10^{13} \text{ cm}^{-3}$, so the Paschen minimal N holds over roughly the scale of the entire cloud, which is likely the most favorable condition for initiation of coronal discharge. If gas kinetic energy is converted to luminescence with, for instance, 2% efficiency, at this density this amounts to $\sim 0.1 \text{ J m}^{-3}$, or 100 J m^{-2} , compared to the Solar Constant (1366 W m^{-2} , with a typical albedo of 7%, yielding 100 W m^{-2}), so might be visible as a color shift for at least several seconds. This argues that a prolonged discharge luminescence effect, including color changes, would require a larger, sustained event (more than the minimal ~ 1 tonne), since the lifetime of some colored TLPs reports is many minutes. It is not reasonable to think that a minimal TLP would sustain a coronal discharge over its entire $\sim 45 \text{ s}$ lifetime sufficient to produce a visible color change.

The timescale predicted for this effect is largely dependent on the assumption that gas is emitted in a single burst. It is plausible that eruption occurs along a non-point source, or that gas is backed up along the length of a channel and produces a prolonged eruption. Additional complications might include the interaction of agitated dust and/or gas with the eruptive channel. Such interactions can also generate large amounts of ionized gases under conditions of moderate voltages e.g., via a mechanism similar to that in a capillaritron (Perel et al. 1981, Bautsch et al. 1994).

These phenomena should also be observable on the nightside surface, too, since solar photoionization is seemingly unimportant in initiating the discharge. At least 20 nightside

TLPs 20 are reported, usually a bright and/or variable spot, 8 at/near Aristarchus e.g., 1824 May 1, near Aristarchus “blinking light, 9th to 10th mag on dark side; 1881 February 3, near Aristarchus: “very bright, like an 8th mag star, pulsating;” 1789 May 29: “flickering spot on east edge of Grimaldi,” etc. A rough calculation of Earthshine lunar surface brightness gives ~ 12 to 13 mag arcsec $^{-2}$ in V, compared to 3.4 mag for full sunlit Moon, so these sources can be relatively faint.

The kernel of many of these ideas has been suggested earlier (Mills 1970), and there is little doubt that luminous electrical discharges are generated in terrestrial volcanic dust clouds (Anderson et al. 1965, Thomas et al. 2007). In general reddish discharges may indicate H α from dissociation of a number of molecular species, although is not the only possible explanation. Note that Kozyrev (1963) reported transient H $_2$ emission from Aristarchus (apparently absent Balmer lines).⁴

Given the suggestion that red events might indicate one of several molecules, it is worth discussing what wavelength range might be best to observe for confirmation. Rather than relying on what might be a bright H α line, plus faint optical lines and bands required to distinguish molecules e.g., CH $_4$ versus H $_2$ O versus NH $_3$, we note that vibrational rotational bands for these (and other molecules) are brighter and more discriminatory in the near-infrared. K-band spectroscopy is likely to produce bright, distinctive features for these and many other molecular candidates, even if only H α might be the only optical transition readily detected.

⁴Kozyrev (1958) obtained another purported TLP spectrum, reportedly showing transient C $_2$ Swan bands.

Appendix II.: Observational and Experimental Techniques

A2.1. Optical/Infrared Remote Sensing

Optical imaging advances several goals. Near Side monitoring for transients recreates how TLPs were originally reported. Not yet knowing their emission mechanism, we should observe them spanning the visual range, 400-700 nm. After an event, longterm changes in the surface morphology and/or photometry might remain. The 0.95 and 1.9 μm surface Fe^{2+} bands and increased blue reflectivity (see above) betray longterm regolith changes.

Hydration is manifest in the infrared. Asteroidal regolith 3 μm hydration signals are common (Lebofsky et al. 1981, Rivkin et al. 1995, 2002, Volquardsen et al. 2004), and stronger than those at 700 nm (Vilas et al. 1999) seen in lunar polar regions. Absorption near 3 μm appears in lunar samples exposed to terrestrial atmosphere for a few years (Markov et al. 1980, Pieters et al. 2005) but not immediately (Akhmanova et al. 1972), and these disappear within a few days in a dry environment. Further sample experiments are needed.

A2.1.1. Earth-Based Imaging

Earth-based monitoring favors the Near Side, but so do TLP-correlated effects: ^{222}Rn outgassing (all four events being nearside, plus most ^{210}Po residual), and mare edges. Optical/IR spatial resolution is limited either by the telescopic diffraction or atmospheric seeing; the best, consistent resolution comes from the *Hubble Space Telescope* with 0.07–0.1 arcsec FWHM (~ 150 m), but with large overhead times due to lunar target/spacecraft motions and instrument setup, requiring ~ 0.5 -1 h in spacecraft time for one filter band. (One arcsecond, a typical optical seeing FWHM, corresponds to 1.8-2.0 km on the Moon, the diffraction limit of a 12 cm telescope at $\lambda = 600$ nm.) Competing high-resolution imaging from “Lucky Exposures” (LE, also “Lucky Imaging”) exploits occasionally superlative imaging within a series of rapid exposures (Fried 1978, Tubbs 2003). Many amateur setups achieve excellent LE results, and the Cambridge group (Law, Mackay & Baldwin 2006) attain diffraction-limited imaging on a 2.5-meter telescope, ~ 200 -300 m FWHM. Only $<1\%$ of observing time survives image selection, but for the Moon this requires little time. LE resolution is limited to a seeing isoplanatic patch, ~ 1000 arcsec², 3000 times smaller than Full Moon. Likewise, *HST*’s Wide Field Camera 3, covering 3000 arcsec², cannot practically survey the Near Side.

High resolution imaging can monitor small areas over time, or in one-shot applications compare imaging with other sources, especially lunar missions. LE or *HST* match the resolution of global maps from *Lunar Reconnaissance Orbiter* Camera’s (LROC) Wide-Angle Camera (Robinson et al. 2005), and *Clementine*/UVIS, over 0.3-1 μm . In comparison, the highest global resolution (*Kaguya* Multiband Imager: Ohtake et al. 2007) has 40-m 2-pixel resolution. LROC’s Narrow Angle Camera has 2 m resolution in one band, targetted.

Chang’e-1/CCD (Yue et al. 2007) might also aid “before/after” sequences. (Note: monitoring TLPs from lunar orbit is detailed in Appendix II.A.) Lunar Orbiter images from 1967, with resolution as good as ~ 1 m, form excellent “before” epochs for many sites, for morphological comparison e.g., of core features of explosive events over several decades.

The prime technique for detecting changes between epochs in similar images is image subtraction. This technique is well-established in studying supernovae, microlensing and variable stars. It produces photon Poisson noise-limited performance (Tomaney & Crotts 1996), is well matched to CCD or CMOS imagers, which at 1-2 arcsec FWHM resolution can cover the whole Moon with 10-20 Mpixels, readily available. One needs at least 2 pixels per FWHM, otherwise non-Poisson residuals tend to dominate.

Our group has automated TLP monitors on the summit of Cerro Tololo, Chile and at Rutherford Observatory in New York that produce regular lunar imaging (Crotts et al. 2009), often simultaneously. Each cover the Near Side at 0.6 arcsec pixel resolution, processed at a rate of one image per 10s. This is sufficient to time-sample nearly all reported TLPs (see Paper I). Image subtraction on these data produces residual images free of systematic errors at nearly Poisson noise levels (Figure 4). (Also we plan a second imaging channel as a video loop, which will record high-speed sequence to be dumped to disk when an TLP alert is triggered.) An imaging monitor opens several possibilities for TLP studies. It produces extensive, objective records of changes in lunar appearance, at sensitivity levels ~ 10 times better than the human eye; an automated system should be able to distinguish changes in contrast at 1% or slightly better, whereas the human eye can only recognize changes of $\gtrsim 10\%$. While we will measure the frequency of TLPs soon enough, Paper I indicates that perhaps one TLP per month might be visible to a human observing at full duty cycle.

Two simultaneous monitors allow imaging a TLP in different bands or polarizations. Dollfus (2000) details TLPs evident as polarimetric anomalies, but on timescales not tightly constrained (6 min to 1 d). Other transient polarimetric events (Dzhapiashvili & Ksanfomaliti 1962, Lipsky & Pospergelis 1966) are even less constrained temporally. These are likely due to scattering linear polarization; one can align the E-vector of one monitor’s polarizer parallel to the Sun-Moon direction on the sky, and a second perpendicular to it. Three or four monitors could reconstruct Stokes parameters for linear polarization conventionally.

TLP imaging monitors open new potential to alert other observers. A monitor detection can trigger LE imaging in a specific active area, or initiate spectroscopic observations to provide information about non-thermal processes and the gas associated with the TLP.

A2.1.2. Ground-Based Spectroscopic/Hyperspectral Observations

Spatially resolved spectroscopy can 1) elucidate the physics of a TLP, including identifi-

cation of gas released, or 2) probe quasi-permanent changes in a TLP site. In order to detect a change, we must make comparisons over a time series, a four-dimensional problem: two spatial dimensions of the lunar surface, plus wavelength, plus time, too much to monitor. One can set a TLP imaging monitor to alert to an event during its duration e.g., in under 1000s, and then point a larger telescope with a spectrograph on the target (within ~ 300 s).

Whereas “hyperspectral” imaging usually refers to a resolving power $R = \lambda/\Delta\lambda \approx 50 - 100$, where $\Delta\lambda$ is the FWHM wavelength resolution, emission lines from TLPs might be many times narrower, thereby diluted at low resolution. If a TLP radiates primarily in line emission, this factor along with our ability to reject photons outside the line profile yields a contrast as high as 10,000 times better than the human eye observing the Moon through a telescope. The IR regolith hydration band near $3.4 \mu\text{m}$ has substructure on the scale of ~ 20 nm, requiring $R \gtrsim 300$. The 950 nm and $1.9 \mu\text{m}$ pyroxene bands show compositional shifts in wavelength centroid and width on the scale of ~ 10 nm (Hazen, Bell & Mao 1978), requiring $R \approx 100$. Differentiating pyroxenes from Fe-bearing glass (Farr et al. 1980) requires $R \approx 50$. In the IR SpeX on the NASA Infrared Telescope Facility can deliver $R \lesssim 2000$.

Observations involve scanning across the lunar face with a long slit spectrograph, greatly improving the contrast of emission-line sources relative to the background (Figure 5). Since spectral reflectance of the lunar surface is largely homogenized by regolith impact mixing, $>99\%$ of the light in such a spectrum is simply “subtracted away” by imposing this average spectrum and looking for deviations from it (Figure 6). The data cube can be sliced in any wavelength to construct maps of lunar features in various bands. Figure 7 shows that specific surface features can be reconstructed in good detail and fidelity.

A2.2. Surface and Subsurface Radar

As in §4, water vapor from the interior might have produced ice within the regolith ~ 10 - 15 m subsurface, a venue for ground-penetrating radar, from Earth or lunar orbit. While epithermal neutrons and gamma radiation can search for hydrogen in permanently shadowed polar crater cold traps, these methods cannot penetrate to these depths. Near the poles or subject to chemical modification (§4.3), ice might range closer to the surface. Past and current lunar radar include *Apollo 17*’s Lunar Sounder Experiment (LSE) (Brown 1972, Porcello 1974) at 5, 16 and 260 MHz, *Kaguya*’s Lunar Radar Sounder (Ono & Oya 2000) at 5 MHz (optionally, 1 MHz or 15 MHz), *LRO*’s Mini-RF (Mini Radio-Frequency Technology Demonstration) on 3 and ~ 10 GHz, and Mini-SAR on *Chandrayaan-1* at 3 GHz (Bussey et al. 2006). For regolith and shallow bedrock, we need frequencies ~ 100 - 300 MHz; LSE operated only a few orbits and near the equator. Near Side maps at ~ 1 km resolution at 430 GHz (Campbell et al. 2007) could improve with intensive ground-based programs, or

from lunar orbit, penetrating ~ 20 m. Orbital missions can combine different frequencies and/or reception angles to improve spatial resolution and ground clutter. Orbital radar can reduce interference speckle noise, otherwise requiring many pointings from Earth.

Earth-based radar is useful; lunar maps exist at 40, 430 and 800 MHz (Thompson & Campbell 2005), also 2.3 GHz (Stacy 1993, Campbell et al. 2006a, b). From Earth large angles of incidence are used e.g., $\sim 60^\circ$, with echoes dominated by diffuse scattering not easily modulated. Circular polarization return measures can test for surface water ice (Nozette 1996, 2001) but are questioned (Simpson 1998, Campbell et al. 2006a). Applying this idea to subsurface ice is at least as problematic. It is unclear that this could be used at the hundreds of MHz required to penetrate to ~ 15 m.

Finding subsurface ice is challenging. The dielectric constant is $K \approx 3$ for both regolith and water ice (which is slightly higher), as for many relevant powders of comparable specific gravity e.g., anorthosite and various basalts. These have attenuation lengths similar to ice, as well. Using of net radar return alone, it will be difficult to distinguish ice from usual regolith by mineral properties. However, in terrestrial situations massive ice bodies reflect little internally e.g., Moorman, Robinson & Burgess (2003). Ice-bearing regions should be relatively dark in radar images, if lunar ice-infused volumes homogenize or “anneal,” either forming a uniform slab or by binding together regolith with ice into a uniform K bulk. On the other hand, hydrated regolith samples have K values much higher than unhydrated ones (by up to 10 times), and attenuation lengths more 10 times shorter (Chung 1972). This hydration effect is largest at lower frequencies, even below 100 MHz. One might expect water ice to perturb regolith chemistry, which might increase charge mobility as in a solution, driving up K and conductivity even more, increasing the loss tangent (conductivity divided by K and frequency). This high- K zone should cause reflections, depending strongly on the details of the suddenness of the transition interface.

Of interest is the 430 MHz radar map (Ghent et al. 2004) of the Aristarchus region, site of $\sim 50\%$ of TLP and radon reports. The 43-km diameter crater is surrounded by a low radar-reflectivity zone some 150 km across, particularly in directions downhill from the Aristarchus Plateau onto Oceanus Procellarum. The Plateau is dark under radar, interrupted by bright craters and Vallis Schröteri. The dark radar halo centered on Aristarchus itself is uniquely smooth, indicating that it was probably formed or modified by the impact, a few hundred My ago. The darkness might be interpreted as high loss tangent, as in the previous paragraph, or simply fewer scatterers (Ghent et al. 2004) i.e., rocks of ~ 1 m size; it is undemonstrated why the latter applies in the ejecta blanket within the bright radar halo within 70 km of the Aristarchus center. Ghent et al. (2005) show that other craters, some comparable in size to Aristarchus, have dark radar haloes, but none so extended. The region around Aristarchus has characteristics potentially expected from subsurface ice redistributed by impact melt:

dark, smooth radar-return, and centered on the impact (although tending downslope). One should search for dark radar areas around likely outgassing sites.

Shorter wavelength radar could map possible changes in surface features due to explosive outgassing, on scales of tens of meters. The *LRO* Mini-RF (Chin et al. 2007) at 4 and 13 cm might easily make such observations. A “before” and “after” radar sequence meshed with optical monitoring may show how outgassing and transients actually alter the regolith.

A2.3. Monitoring from Low Lunar Orbit

Alpha-Particle Spectrometry: A ^{222}Rn atom random walks only ~ 200 km before decaying (or sticking to a cold surface). Unless detected in under a day, ^{222}Rn dispersal makes superfluous placing detectors < 100 km above the surface (excepting r^{-2} sensitivity considerations).

Several alpha-particle spectrometers have observed the Moon, successfully for short periods. The latitude coverage was limited on *Apollo 15* ($| \text{Lat} | \lesssim 26^\circ$ for 145 hours) and *Apollo 16* ($| \text{Lat} | \lesssim 5^\circ$, 128 h). *Lunar Prospector’s* Alpha Particle Spectrometer covered the entire Moon, over 229 days spanning 16 months, but was partially damaged (one of five detectors) upon launch and suffered a sensitivity drop due solar activity (Binder 1998). *Kaguya’s* Alpha Ray Detector (ARD) was designed with 25 times more sensitivity than the Apollo instruments (Nishimura et al. 2006), but shared a failed power supply and has yet to produce results. *Apollo 15* observed two outgassing events (from Aristarchus and Grimaldi), *Apollo 16* none, and *Lunar Prospector* two sources (Aristarchus and Kepler) integrated over the mission duration. Apollo and *Lunar Prospector* detected enhanced decay product ^{210}Po at mare/highlands boundaries from ^{222}Rn leakage over the past ~ 100 y. The expected detection rate, for a single alpha-particle spectrometer in a polar orbit and without instantaneous sensitivity problems, might be grossly estimated from these data, consistent with Aristarchus producing an outgassing event 1-2 times per month at the level detectable by *Apollo 15*, and by *Lunar Prospector* when integrated over the mission, with sites such as Grimaldi and Kepler collectively produce events roughly equally with Aristarchus. A new orbiting alpha-particle spectrometer with a lifetime of a year or more and an instantaneous sensitivity equal to that of *Apollo 15’s* detector would likely produce a relatively detailed map of where outgassing occurs on the lunar surface, separate from any optical manifestation. orbits would cover the lunar surface every 1.8 half-lives of ^{222}Rn . This may nearly double the detected sample. Sensitivity can be increased if alpha-particle detectors incorporate a veto for solar wind particles, or operate during solar minimum (starting next in 2016), and if detectors can be kept oriented towards the lunar surface.

On-Orbit Mass Spectrometry: The long surface residence of ^{222}Rn allows alpha-particle detection and localization at high efficiency with even one orbital instruments. This is untrue

of prompt detection of outgassing events e.g., by mass spectrometry. With outgassing of hundreds of tons and tens of events per year, particle mass fluence from one outburst seen 1000 km away approaches 10^{12} AMU cm^{-2} . A burst that can be seen by a few detectors would be very well constrained. With gas scale heights ~ 100 km one needs detectors near the ground. (We describe briefly possible orbits in Appendix II.B.) On the other hand, an instantaneous outburst seen 100 km away will disperse less than one minute in arrival; detectors must operate on short time intervals. This has been a problem e.g., the *Apollo 15* Orbital Mass Spectrometer Experiment (Hoffman & Hodges 1972), requiring 62s to scan through a factor of 2.3 in mass. Clearly there are also two separate modes for gas propagation above the lunar surface, neutral and ionized, are significant (Vondrak, Freeman & Lindeman 1974, Hodges et al. 1972), at rates of one to hundreds of tonne y^{-1} for each process.

Specific operational strategies of these detectors is paramount. Consider an event at 1000 km distance, which will spread ~ 500 s in arrival time. A simple gas pressure gauge will be insufficiently sensitive; with an ambient atmosphere not atypical e.g., number density $n \approx 10^4 - 10^5 \text{ cm}^{-3}$ (varying day/night e.g., Hodges, Hoffman & Johnson 2000), the collisional background rate in 500 s amounts to $10\times$ or more than the fluence for a typical outburst (assuming ~ 20 AMU particles). Since interplanetary solar proton densities can change by amount of order unity in an hour or less (e.g., McGuire 2006), pressure alone is insufficient. Mass spectrometry helps by subdividing incoming flux, in mass, obviously, but also in direction, thus decreasing effective background rates.

There is degeneracy in timing recorded by a satellite particle detector between episodic behavior of particle outgassing versus motion of the spacecraft at $\sim 1.7 \text{ km s}^{-1}$. Localizing such signals between two platforms is ideal, at least for neutral species. Outgassing detectors on each platform would constrain temporal/spatial location of specific outbursts using differences in timing and signal strength. The timing difference indicates the distance difference to the sources, with the source confined to a hyperboloid locus. Location on this hyperboloid is fixed by signal strengths, plus left/right ambiguity from detector directionality. Maintaining a mean nearest satellite distance of 1000 km from arbitrary sources requires $\gtrsim 10$ low orbital platforms. Mass spectrometers on the surface can maintain such density over smaller areas efficiently once we know roughly where sources may be. A mass spectrometer planned for *Lunar Atmospheric and Dust Environment Explorer (LADEE)* sits on one platform in equatorial orbit; geographical resolution of outgassing events will be poor.

A2.4. In-Situ and Near Surface Exploration

Detailing all possible *in situ* approaches to studying volatiles is beyond the scope of this paper. (Our research group, AEOLUS: “Atmosphere seen from Earth, Orbit and the LUnar

Surface,” is developing ways to efficiently transfer information from remote sensing to *in situ* research of lunar volatiles.) We emphasize a few key points. The key effort is to focus from wide-ranging reconnaissance down to scales where lunar volatiles can be sampled near their source. Primary strategies one might choose for global surveys are optical transient monitoring (Near Side only, resolution ~ 1 km), and, for direct detection of outgassing, orbital ^{222}Rn detection (both hemispheres, ~ 100 km resolution). Even trusting that TLPs trace volatiles, and centroiding TLPs to 10% of a resolution element, localization error (~ 100 m) might easily preclude easy *in situ* followup. (In Appendix II.A we outline how this might improve to ~ 10 m.) Two simple *in situ* technologies could further isolate outgassing sources below 100 km scales. First, alpha particle spectrometers can be placed on the surface and three used to triangulate ^{222}Rn outgassing sources within a few hundred km of the instruments, using strength and time delay in the arrival of random walking radon. Secondly, a mass spectrometer that can reconstruct the ballistic trajectory of neutrals from the source (Austin et al. 2008, Daly, Radebaugh & Austin 2009) can construct an “image” of the transient outgassing sources over a region as large as 1000 km across. This spectrometer is not overwhelmed by pulsed sources while measuring masses over a wide range. There are several technologies which might allow to pinpoint subsurface structures on the 10 m level from information at 1 km scales: local seismic arrays, local ground penetrating radar, magnetometer arrays, and infrared laser arrays. The latter would consist of lasers and mirrors on towers that would be sensitive to specific molecular species and could either be constructed to exploit a specific species e.g., CO_2 , or tuned to select one of several species’ vibrational-rotational states. On even smaller scales (1-100 m) several varieties of mass spectroscopy might prove effective, including downward-sniffing spectrometers, triangulating outburst detectors arrays, and pyrolysis mass spectrometers (ten Kate et al. 2009) which heat regolith samples in search of absorbed species from previous outgassing episodes.

By LACE’s deployment with the final Apollo landing, the outgassing environment was significantly contaminated by anthropogenic gas (Freeman & Hills 1991) especially near landing sites; each mission of human exploration will deliver tens of tonnes gases to the surface, with species relevant to endogenous volcanic gas, approaching or exceeding the annual endogenous output of such gases. Constellation spacecraft Orion burn N_2O_4 (nitrogen tetroxide) and $\text{CH}_3\text{N}_2\text{H}_3$ (mono-methyl hydrazine), with Altair propelled by liquid oxygen and hydrogen. (Future missions might use liquid O_2 and CH_4 . Earth Departure Stages might deliver residual O_2 and H_2 in lunar impact.) Altair (and EDS) produce water, and Orion exhausts H_2O , CO_2 and N_2 . (N_2 was the prime candidate constituent in an outburst seen by the *Apollo 15* over Mare Orientale: Hoffman & Hodges 1972, perhaps anthropogenically - Hodges 1991.) Depending on spacecraft orientations and trajectories when thrusting they may deliver ~ 20 tonnes of mostly water to the surface, where most will remain up to about one lunation, making suspect measurements of these and other species for years.

Appendix II.A: Imaging from High Orbit

With the constraints on imaging from Earth, it is interesting to consider the limits and potentials of imaging monitors closer to the Moon. We will not propose special-purpose missions in space-based remote sensing. (We could mention dedicated missions related to in-situ exploration of areas affected by volatiles, where special-purpose investment seems unavoidable. We postpone this to later work.) We discuss experiments and detectors which might ride on other platforms, preceding or in concert with human exploration, which will accommodate the orbits and mission parameters which might be chosen for other purposes.

An instance of such joint use: does exploration of the Moon imply establishment of a communications network with line-of-sight visibility from essentially all points on the lunar surface (excepting those within deep craters, etc.)? If so, these platforms might also serve as suitable locations for comprehensive imaging monitoring. A minimal network might have a tetrahedral configuration with points ~ 60000 km above the surface: a single platform at Earth-Moon Lagrange point L1, covering most of the Near Side, and three points in wide halo orbits around L2, covering their respective portions of the Far Side plus a portion of the limb as seen from Earth. Discussion is underway of an L1 facility to aid in orbital transfer throughout the Solar System (Lo 2004, Ross 2006). No single satellite can cover the entire Far Side, especially farside radio astronomy restricts low-frequency communications e.g., lasers only. A single L2 satellite can cover at most 97% of the Far Side (subtending $176^\circ.8$, selenocentrically); full coverage (plus some communications redundancy) requires three satellites, plus a means of covering the Near Side. With this configuration, the farthest point from a satellite will be typically 71° (in selenocentric angle), hence foreshortened due to proximity to the limb by ~ 3 times.

An imaging monitor to improve significantly on Earth-vicinity capabilities might need to be an ambitious undertaking. To achieve 100m FWHM resolution at the sub-satellite point on the Moon surface requires an imager of ~ 4 Gpixels, an aperture $\gtrsim 0.5$ m, and a field-of-view of $3^\circ.3$. Each such monitor, separate from power, downlink, attitude control and other infrastructure requirements will cost perhaps \$100M. Perhaps the system could be cut to a single farside monitor, in a narrow halo orbit extending beyond the Moon's Earth-shadow, plus some nearside monitoring, which together could still cover perhaps 95% of the lunar surface, albeit with some extreme limb foreshortening. We also need to ask ourselves at some point whether essential research and resource exploitation might be confined to the Near Side. If the goal is to discover the source of volatiles for the sake of further scientific exploration or resource exploitation, however, an investment in remote sensing, in terms of spatial resolution makes in-situ reconnaissance and exploration much less problematic. In the meantime, we should accomplish what is possible from the ground.

Appendix II.B: Low-Maintenance and Sun-Synchronous Low Orbits

It is also worth mentioning what might be done for polar or nearly-polar low orbits, for techniques described in §6.3 and 6.4. For a low lunar orbit to be “low maintenance” i.e., require few corrections due to mascon perturbations, it should be at one of several special “frozen orbit” inclination angles $i = 27^\circ, 50^\circ, 76^\circ$ or 86° (e.g., Ramanan & Adimurthy 2005). However, we want to maintain a position over the terminator, using a sun-synchronous orbit, which requires a precession rate $\omega_p = 0.99^\circ d^{-1} = 2 \times 10^{-7} \text{ rad s}^{-1}$. Alternatively, LADEE achieves this by a precessing, highly eccentric orbit, but spends a small fraction of its time near the lunar surface. Natural precession due to lunar oblateness is determined by the gravitational coefficient $J_2 = (2.034 \pm 0.001) \times 10^{-4}$ (Konopliv et al. 1998) according to $\omega_p = -(3a^2 J_2 \omega \cos i)/(2r^2) = -(3a^2 J_2 \sqrt{GM} \cos i)/(2r^{7/2})$, where a is the lunar radius, ω the orbital angular speed, M the lunar mass and r the orbital radius. (The precession caused by Earth is 1000 times smaller, and 60000 times smaller for the Sun.) One cannot effectively institute both conditions, however, since the maximum inclination orbit with $\omega_p = 2 \times 10^{-7} \text{ s}^{-1}$ occurs at 47° (or else the orbit is below the surface). While an orbit at $i = 27^\circ$ is stable (at $r = 1876 \text{ km}$, 138 km above the surface) and has the correct precession rate, it spends most of its time away from the terminator.

In contrast, at $i = 87^\circ$, $\omega_p = 1.5 \times 10^{-8} \text{ s}^{-1}$, and the spacecraft needs to accelerate continuously only $a = 0.3 \text{ mm s}^{-2}$ to place it into sun-synchronous precession. This is nearly the same as the thrust provided by the Hall-effect ion engine on *SMART-1* (and corresponds to an area per mass of $330 \text{ cm}^2 \text{ g}^{-1}$ under the influence of solar radiation pressure.) While it is not apparent that an ion engine would be the best choice for a platform with mass and ion spectrometers, this illustrates the small amount of impulse need to maintain this favorable orbit, comparable to station-keeping in many non-frozen orbits. In truth, the most efficient location to apply this acceleration is only near the poles, so a slightly more powerful thruster might be needed. Since, time-averaged, this perturbed orbit still lands in a frozen-orbit zone, it should still be relatively stable in terms of radius. An instrumented platform in this driven, sun-synchronous polar orbit would be ideal for studying outgassing signals near the terminators.

References:

- Adams, J.B. 1974, JGR, 79, 4829.
- Adorjan, A.S. 1970, J. Spacecraft & Rockets, 7, 378.
- Akhmanova, M.V., Dement'yev, B.V. & Markov, M.N. 1978, Geokhimiya, 2, 285.
- Akhmanova, M.V., Dement'yev, B.V., Markov, M.N. & Sushchinskii, M.M. 1972, Cosmic Res., 10, 381
- Allen, C.C., et al. 1998, Lun. Plan. Sci. Conf., 29, 1690.
- Anders, E. 1970, Science, 169, 1309.
- Anders, E. Ganapathy, R., Krähenbühl, U. & Morgan, J.W. 1973, The Moon, 8, 3.
- Anderson, R.. et al. 1965, Science, 148, 1179.
- Andreas 2007, Icarus, 286, 24.
- Austin, D.E., Miller, I., Daly, T., Crotts, A., Syrstad, E., Brinckerhoff, W. & Radebaugh, J. 2008, NLSI Lun. Sci. Conf., 2074.
- Bart, G.D. & Melosh, H.J. 2005, D.P.S., 57, 57.07.
- Bautsch, M., Varadinek, P., Wege, S. & Niedrig, H. 1994, J. Vac. Sci. Technol. A., 12, 591.
- Basu, A. & Molinaroli, E. 2001, Earth Moon & Plan., 85, 25.
- Brantley, S.L. 2004, in “Treatise on Geochemistry” eds. H.D. Holland & K.K. Turekian (Elsevier: Amsterdam), section 5.03.
- Brown, W.E., Jr. 1972, Earth Moon Plan., 4, 133.
- Buratti, B.J., McConnochie, T.H., Calkins, S.B., Hillier, J.K. & Herkenhoff, K.E. 2000, Icarus, 146, 98.
- Bussey, B., Spudis, P.D., Lichtenberg, C., Marinelli, B. & Nozette, S. 2006, in *LCROSS Selection Conf.*, (LPI: Houston), 9013.
- Cameron, W.S. 1972, Icarus, 16, 339.
- Cameron, W.S. 1977, Phys. Earth Planet. Inter., 14, 194.
- Campbell, B.A., Campbell, D.B., Margot, J.-L., Ghent, R.R., Nolan, M., Carter, L.M., Stacy, N.J.S. 2007, Eos, 88, 13.
- Campbell, D.B., Campbell, B.A., Carter, L.M., Margot, J.-L. & Stacy, N.J.S. 2006a, Nature,

443, 835.

Campbell, B.A., Carter, L.M., Campbell, D.B., Hawke, B.R., Ghent, R.R. & Margot, J.-L. 2006b, *Lun. Plan. Sci. Conf.*, 37, 1717.

Carbognani, A. 2004, *Astronomia*, 5, 12.

Carrier, W.D., Olhoeft, G.R. & Mendell, W. 1991, in “Lunar Sourcebook,” eds. G.H. Heiken, D.T. Vaniman & B.M. French (Cambridge U.: Cambridge), p. 475.

Charette, M.P., Adams, J.B., Soderblom, L.A., Gaffey, M.J. & McCord, T.B. 1976, *Lun. Sci. Conf.*, 7, 2579.

Charles, R.W., Hewitt, D.A. & Wones, D.R. 1971, *Lun. Sci. Conf.*, 1, 645.

Chevrier, V., et al. 2007, *GRL*, 34, L02203.

Chin, G., et al. 2007, *Lun. Plan. Sci. Conf.*, 38, 1764.

Chung, D.H. 1972, *Earth Moon & Plan.*, 4, 356.

Cocks, F.H., et al. 2002, *Icarus*, 160, 386.

Collins, G.S. 2001, *Lun. Plan. Sci. Conf.*, 32, 1752.

Compton, K.T., Lilly, E.G. & Olmstead, P.S. 1920, *Phys. Rev.*, 16, 282.

Crotts et al. 2009, in preparation.

Crotts, A.P.S. 2008, *ApJ*, 687, 1186.

Crotts, A.P.S. 2009, *ApJ*, 697, 1.

Cullingford, H.S. & Keller, M.D. 1988, in *2nd Conf. on Lunar Bases and Space Activities*, ed. W.W. Mendell, NASA Conf. Pub. 3166, p. 497.

Daly, T., Radebaugh, J. & Austin, D.E. 2009, *Lun. Plan. Sci. Conf.*, 40, 2411.

Davis, S.S. 2009, *Icarus*, 202, 383.

Dollfus, A. 2000, *Icarus*, 146, 430.

Drake, M.J. & Stimpfl, M. 2007, *Lun. Plan. Sci. Conf.*, 38, 1179.

Dzhapiashvili, V.P. & Ksanfomaliti, L.V. 1962, *The Moon*, IAU Symp. 14, (Academic Press: London), p. 463.

Elkins-Tanton, L.T., Chatterjee, N. & Grove, T.L. 2003, *Meteor. & Plan. Sci.*, 38, 515.

Epstein, S. & Taylor, H.P., Jr. 1972, *Geochim. Cosmochim. Acta*, 36 (Suppl. 3), 1429.

- Farmer, C.B. 1976, *Icarus*, 28, 279.
- Farrell, W.M., Plaut, J.J., Gurnett, D.A. & Picardi, G. 2005, *GRL*, 32, L11204.
- Farr, T.G., Bates, B., Ralph, R.L. & Adams, J.B. 1980, *Lun. Plan. Sci.*, 11, 276.
- Freeman, J.W., Jr. & Hills, H.K. 1991, *GRL*, 18, 2109.
- Fried, D.L. 1978, *Opt. Soc. Am. J.*, 68, 1651.
- Friesen, L.J. 1975, *The Moon*, 13, 425.
- Gammage, R.B. & Holmes, H.F. 1975, *Lun. Sci. Conf.*, 6, 3305.
- Garlick, G.F.J., Steigmann, G.A. & Lamb, W.E. 1972a, *Nature*, 238, 13.
- Garlick, G.F.J., Steigmann, G.A., Lamb, W.E. & Geake, J.E. 1972b, 1972, *Lun. Plan. Sci. Conf.*, 3, 2681.
- Garvin, J., Robinson, M., Skillman, D., Pieters, C., Hapke, B. & Ulmer, M. 2005, *HST* Proposal GO 10719.
- Gault, D.E., Hörz, F, Brownlee, D.E. & Hartung, J.B. 1974, *Lun. Plan. Sci. Conf.*, 5, 260.
- Geake, J.E. & Mills, A.A. 1977, *Phys. Earth Planet. Inter.*, 14, 299.
- Gerlach, T.M. & Graeber, E.J. 1985, *Nature*, 313, 274
- Ghent, R.R., Leverington, D.K., Campbell, B.A., Hawke, B.R. & Campbell, D.B. 2004, *Lun. Plan. Sci. Conf.*, 35, 1679.
- Ghent, R.R., Leverington, D.K., Campbell, B.A., Hawke, B.R. & Campbell, D.B. 2005, *JGR*. 110, doi: 10.1029/2004JE002366.
- Gibson, E.K. & Moore, G.W. 1973, *Science*, 179, 69.
- Hauri, E.H., Saal, A.E., van Orman, J.A., Rutherford, M.C. & Friedman, B. 2009, *Lun. Plan. Sci. Conf.*, 40, 2334.
- Haynes, D.R., Tro, N.J. & George, S.M. 1992, *J. Phys. Chem.*, 96, 8502.
- Hazen, R.M., Bell, P.M. & Mao, H.K. 1978, *Lun. Plan. Sci.*, 9, 483.
- Hodges, R.R., Jr. 1977, *Phys. Earth & Planet. Inter.*, 14, 282.
- Hodges, R.R., Jr. 1980, *Proc. Lun. Plan. Sci. Conf.*, 11, 2463.
- Hodges, R.R., Jr. 1991, *personnel communication*, in Stern, A. 1999, *Rev. Geophys.*, 37, 4.
- Hodges, R.R., Jr., Hoffman, J.H., Yeh, T.T.J. & Chang, G.K. 1972, *JGR*, 77, 4079

- Hodges, R.R., Jr., Hoffman, J.H., Johnson, F.S. & Evans, D.E. 1973, Lun. Sci. Conf., 4, 2855.
- Hodges, R.R., Jr., Hoffman, J.H. & Johnson, F.S. 1974, Icarus, 21, 415.
- Hodges, R.R., Jr. & Hoffman, J.H. 1975, Lun. Plan. Sci. Conf., 6, 3039.
- Hoffman, J.H. & Hodges, R.R., Jr. 1975, Moon, 14, 159.
- Horiguchi, T., Saeki, N., Yoneda, T., Hoshi, T. & Lin, T.D. 1996, in “Space V: 5th Internat’l Conf. Engin., Constr. & Operat. in Space,” ed. S.W. Stewart, ASCE Proc., 207, 86.
- Horiguchi, T., Saeki, N., Yoneda, T., Hoshi, T. & Lin, T.D. 1998, in “Space ‘98: 6th Internat’l Conf. Engin., Constr. & Operat. in Space,” eds. R.G. Galloway & S.L. Lokaj, ASCE Proc., 206, 65.
- Hughes, D.W. 1980, Nature, 285, 438.
- Ingersoll, A.P. 1970, Science, 168, 972.
- Kanamori, H. in *Concrete Under Severe Conditions 1: Environment and Loading*, eds. K. Sakai, N. Banthia & O.E. Gjorv (Chapman & Hall: London), p. 1283.
- Kozyrev, N.A. 1958, Sov. Intern’t’l Geop. Yr. Bull., PB 13162-42 (see also 1962, in *The Moon, IAU Symp. 14*, eds. Z. Kopal & Z.K. Mikhailov (Academic: New York), p. 263.
- Kozyrev, N.A. 1963, Nature, 198, 979.
- Krähenbühl, U., Ganapathy, R., Morgan, J.W. & Anders, E. 1973, Science, 180, 858.
- Langseth, M.G., Jr., Clarke, S.P., Jr., Chute, J.L., Jr., Keihm, S.J. & Wechsler, A.E. 1972, in *Apollo 15 Preliminary Science Report*, NASA SP-289, p. 11-1.
- Langseth, M.G., Jr., Keihm, S.J. & Chute, J.L., Jr. 1973, in *Apollo 17 Preliminary Science Report*, NASA SP-330, p. 9-1.
- Langseth, M.G. & Keihm, S.J. 1977, in *Soviet-American Conference on Geochemistry of the Moon and Planets*, NASA SP-370, p. 283.
- Law, N.M., Mackay, C.D. & Baldwin, J.E. 2006, A&A, 446, 739.
- Lebofsky, L.A., Feierberg, M.A., Tokunaga, A.T., Larson, H.P. & Johnson, J.R. 1981, Icarus, 48, 453
- Lipsky, Yu.N. & Pospergelis, M.M. 1966, Astronomicheskii Tsirkular, 389, 1.
- Lo, M.W. 2004, in “Proc. Internat’l Lunar Conf. 2003, ILEWG 5” (Adv. in Astronaut. Sci., Sci. & Tech. Ser., Vol. 108), eds. S.M. Durst et al. (Univelt: San Diego), p. 214.

- Lucey, P.G., Blewett, D.T., Taylor, G.J. & Hawke, B.R. 2000, JGR, 105, 20377.
- Lucey, P.G., Taylor, G.J. & Hawke, B.R. 1998, Lun. Plan. Sci. Conf., 29, 1356.
- Lunine, J., Graps, A., O’Brien, D.P., Morbidelli, A., Leshin, L. & Coradini, A. 2007, Lun. Plan. Sci. Conf., 28, 1616.
- Markov, M.N., Petrov, V.S., Akhmanova, M.V. & Dementev, B.V. 1979, in *Space Research, Proc. Open Mtgs. Working Groups* (Pergamon: Oxford), p. 189.
- Martin, R.T., Winkler, J.L., Johnson S.W. & Carrier, III, W.D. 1973, “Measurement of conductance of Apollo 12 lunar simulant taken in the molecular flow range for helium, argon, and krypton gases.” Unpublished report quoted in Carrier et al. (1991).
- McCubbin, F.M., Nekvasil, H. & Lindsley, D.H. 2007, Lun. Plan. Sci. Conf., 38, 1354.
- McEwen, A.S., Robinson, M.S., Eliason, E.M., Lucey, P.G., Duxbury, T.C. & Spudis, P.D. 1994, *Science*, 266, 1858.
- McKay, D.S., Fruland, R.M. & Heiken, G.H. 1974, Lun. Plan. Sci. Conf., 5, 887.
- McKay, D.S., et al. 1991, in “Lunar Sourcebook,” eds. G.H. Heiken, D.T. Vaniman & B.M. French (Cambridge U. Press: Cambridge), p. 285.
- Middlehurst, B.M. 1977, Roy. Soc. Phil. Trans. A, 285, 485.
- Mills, A.A. 1969, *Nature*, 224, 863
- Mills, A.A. 1970, *Nature*, 225, 939.
- Moorman, B.J., Robinson, S.D. & Burgess, M.M. 2003, *Permafrost & Periglac. Proc.*, 14, 319.
- Morgan, T.H. & Shemansky, D.E. 1991, JGR, 96, 1351.
- Mukherjee, N.R. 1975, *The Moon*, 14, 169.
- Neukum, G., et al. 2001, *Space & Sci. Rev.*, 96, 55.
- Nozette, S. et al. 1996, *Science*, 274, 1495.
- Nozette, S. et al. 2001, JGR, 106, 23253.
- O’Hara, M.J. 2000, *J. Petrology*, 41, 11, 1545.
- Ohtake, M. et al. 2007, Lun. Plan. Sci. Conf., 38, 1829.
- Ono, T. & Oya, H. 2000, *Earth Plan. Space*, 52, 629.

- Pearse, R.W.B. & Gaydon, A.G. 1963, *The Identification of Molecular Spectra*, (Ugsmann & Hall: London)
- Perel, J., Mahoney, J.F., Kalensher, B.E. & Forrester, A.T. 1981, Appl. Phys. Lett., 38, 320.
- Pieters, C.M., et al. 2005, <http://moonmineralogymapper.jpl.nasa.gov/SCIENCE/Volatiles/>
- Pieters, C. et al. 2006, Lun. Plan. Sci. Conf., 37, 1630.
- Porcello, L.J., et al. 1974, Proc. IEEE, 62, 769.
- Quaide, W. & Oberbeck, V. 1975, Moon, 13, 27.
- Reader, J. & Corliss, C.H. 1980, CRC Handbook of Chemistry & Physics, 68.
- Rivkin, A.S., Howell, E.S., Britt, D.T., Lebofsky, L.A., Nolan, M.C. Branston, D.D. 1995, Icarus, 117, 90
- Rivkin et al. 2002, Asteroids III, 237
- Robinson, J.H. 1986, JBAA, 97, 12.
- Robinson, M.S. et al. 2005, Lun. Plan. Sci. Conf., 36, 1576.
- Ross, S.D. 2006, Am. Sci., 94, 230.
- Rubey, W.W. 1964, in “Origin & Evolution of Atmospheres & Oceans,” eds. P.J. Brancazio & A.G.W. Cameron (Wiley: New York), p. 1.
- Rutherford, M.J. & Papale, P. 2009, Geology, 37, 219.
- Saito, Y., Tanaka, S., Takita, J., Horai, K. & Hagermann, A. 2007, Lun. Plan. Sci. Conf., 38, 2197.
- Sato, M. 1976, Proc. Lun. & Plan. Sci. Conf., 7, 1323.
- Sato, M. 1979, Proc. Lun. & Plan. Sci. Conf., 10, 311.
- Saal, A.E., Hauri, E.H., Cascio, M.L., van Orman, J.A., Rutherford, M.C. & Cooper, R.F. 2008, Nature, 454, 192.
- Schorghofer, N. & Taylor, G.J. 2007, JGR, 112, E02010.
- Schultz, P.H., Staid, M.I. & Pieters, C.M. 2006, Nature, 444, 184.
- Schumm, S.A. 1970, Geol. Soc. Amer. Bull., 81, 2539.
- Shearer, C.K., Layne, G.D. & Papike, J.J. 1994, Geochim. CosmoChim. Acta, 58, 5349.
- Siegal, B.S. & Gold, D.P. 1973, Moon, 6, 304.

- Simpson, R.A. 1998, in “Workshop on New Views of the Moon,” eds. B.L. Jolliff & G. Ryder (LPI: Houston), p. 61.
- Speedy, R.J., Denebetti, P.G., Smith, R.S., Huang, C. & Kay, B.D. 1996, *J. Chem. Phys.*, 105, 240.
- Spohn, T., Konrad, W., Breuer, D. & Ziethe, R. 2001, *Icarus*, 149, 54.
- Spudis, P.H. & Schultz, P.D. 1983, *Nature*, 302, 233.
- Stacy, N.J.S. 1993, Ph.D. thesis (Cornell U.).
- Stern, A. 1999, *Rev. Geophys.*, 37, 4.
- Stimpfl, M., de Leeuw, N.H., Drake, M.J. & Deymier, P. 2007, *Lun. Plan. Sci. Conf.*, 38, 1183.
- Stubbs, V.J., Vondrak, R.R. & Farrell, W.H. 2005, *Lun. Plan. Sci. Conf.*, 36, 1899.
- Taylor, S.R. 1975, *Lunar Science: a Post-Apollo View* (Pergamon: NY), 372 pp.
- ten Kate, I.L., Glavin, D.P. & the VAPoR team, *Lun. Plan. Sci. Conf.*, 40, 2232.
- Thomas, G.E. 1974, *Science*, 183, 1197.
- Thomas, R.J., et al. 2007, *Science*, 315, 1097.
- Thompson, T.W. & Campbell, B.A. 2005, *Lun. Plan. Sci. Conf.*, 36, 1535.
- Tomaney, A. & Crotts, A.P.S. 1996, *AJ*, 112, 2872.
- Tubbs, R.N. 2003, Ph.D. thesis (University of Cambridge).
- Volquardsen, E.L., Rivkin, A.S. & Bus, S.J. 2004, *DPS*, 36, 32.13.
- Vondrak, R.R., Freeman, J.W. & Lindeman, R.A. 1974, *Lun. & Plan. Sci. Conf.*, 5, 2945.
- Washburn, E., et al., eds. 2003, *International Critical Tables of Numerical Data, Physics, Chemistry and Technology* (Knovel: Norwich, NY), elec. edition.
- Williams, R.J. & Gibson, E.K. 1972, *Earth Plan. Sci. Let.*, 17, 84.
- Wilson, L. & Head, J.W. 2003, *Geophys. Res. Let.*, 30, 1605.
- Yue, Z., Xie, H., Liu, J. & Ouyang, Z. 2007, *Lun. Plan. Sci. Conf.*, 38,
- Zito, R.R. 1989, *Icarus*, 82, 419.

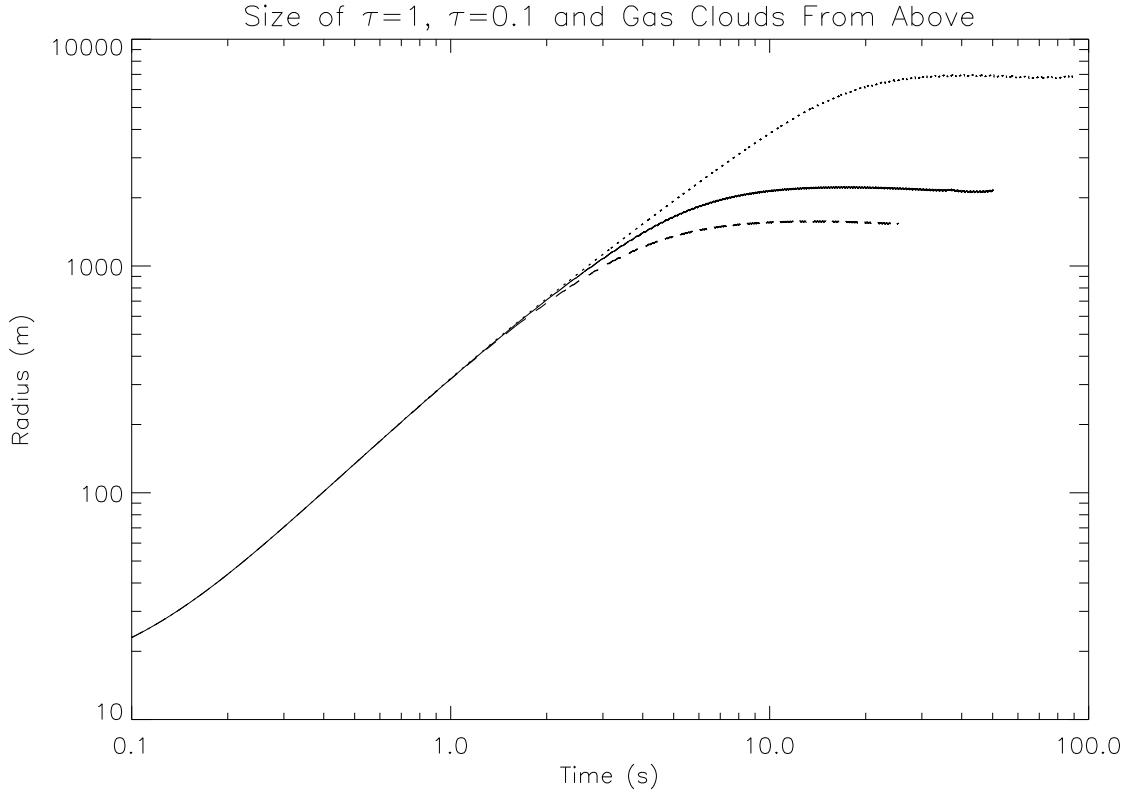


Fig. 1.— The size of the various components of the clouds as seen from above, versus time after the initial explosion, for a “minimal TLP.” The solid line represents the radius of the dust cloud with optical thickness $\tau = 1$ as seen from above. The dotted line represents the radius of the dust cloud with $\tau = 0.1$ as seen from above. These two optical depth values correspond roughly to the level of change in contrast that might be considered easy versus marginal to detect with the human eye observing lunar surface features affected by the event. The dashed line represents the radius of the outermost layer of the gas cloud still constrained by the dust cloud. At 25 s after the explosion, the $\tau = 1$ portion of the cloud has expanded to 2 km radius, after which time no portion of the cloud remains with $\tau = 1$. After 90 s, the $\tau = 0.1$ portion of the cloud has also disappeared, having first expanded to 7 km in radius.

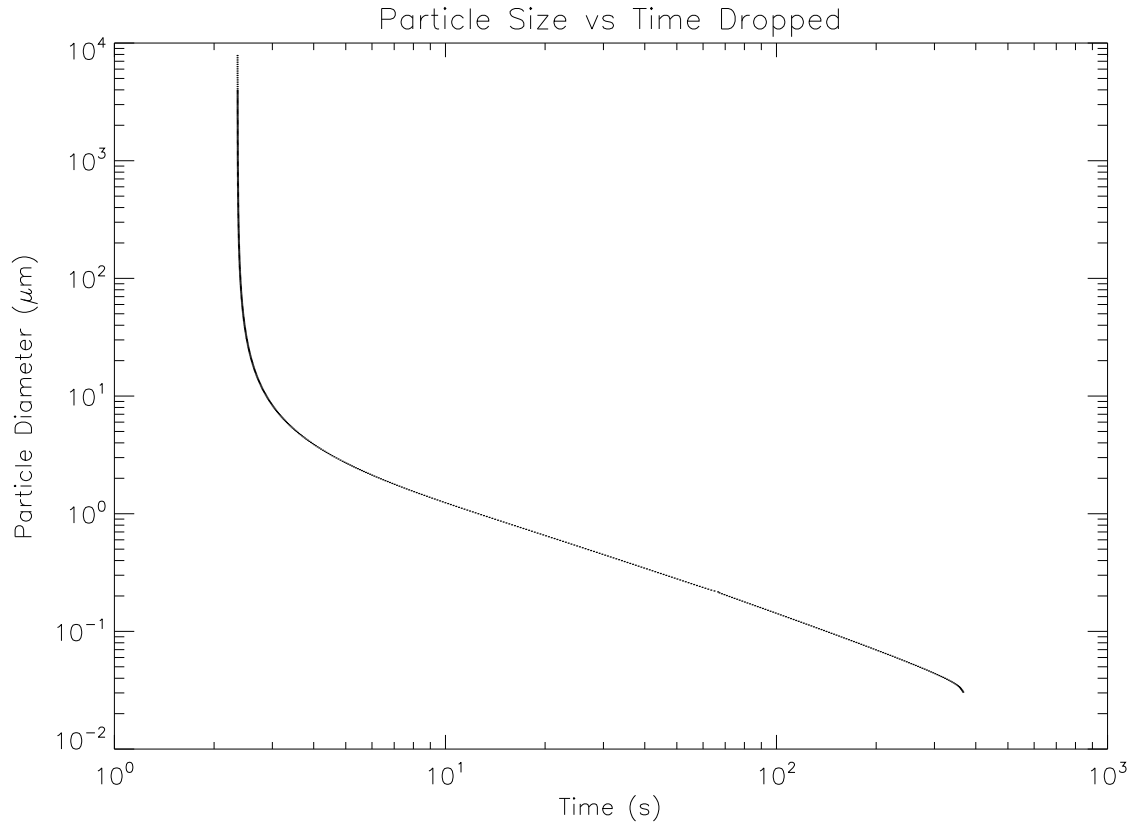


Fig. 2.— The time required for a typical regolith particle of the diameter shown to fall out of the expanding cloud back to the lunar surface. Particles larger than about 10 micron (more than 50% by mass) rain immediately to the ground, whereas particles smaller than optical wavelength remain aloft for at least several minutes.

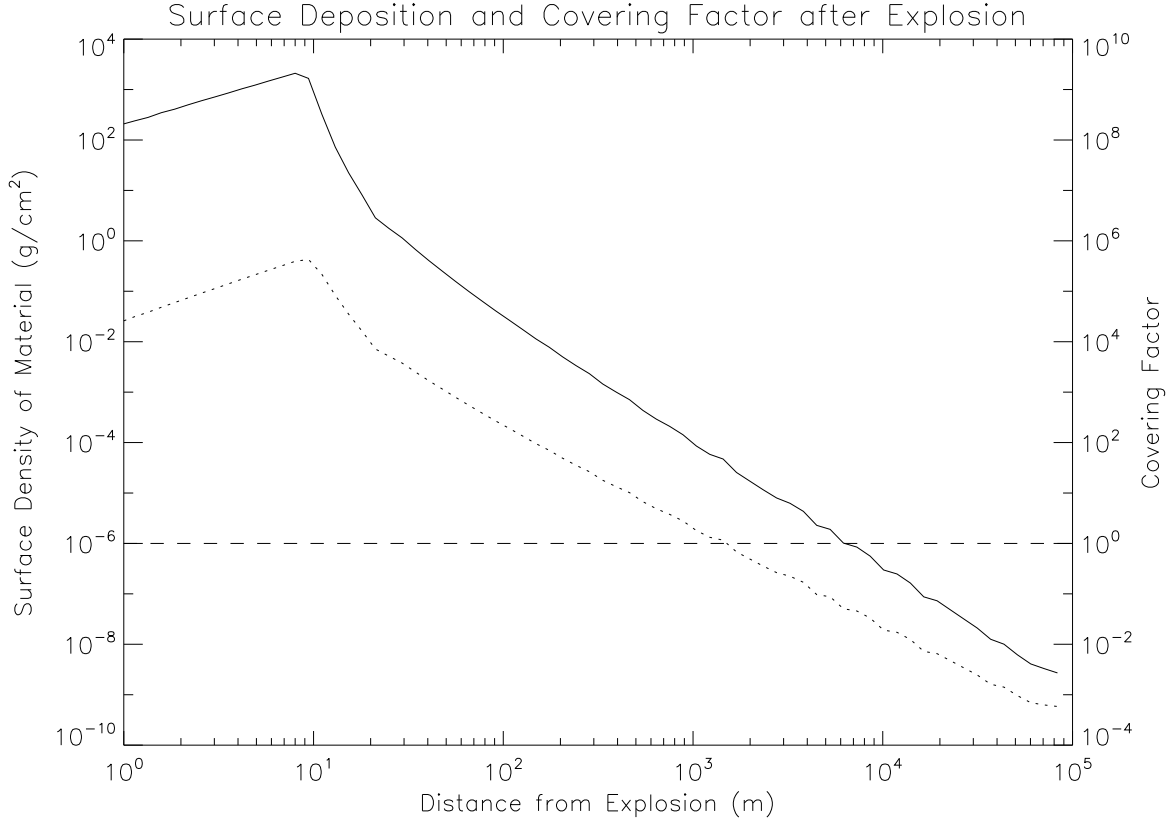


Fig. 3.— The surface density and covering factor of material deposited by our model “minimal TLP” versus the distance from the explosion center. The surface density (mass per unit area) is the solid curve and covering factor (total projected particle area per unit area) is dotted, with unit coverage denoted by the dashed line. Away from the crater, there is a near power-law of exponent -2.6 for the surface density of regolith deposited as a function of radius. The maximum found at $r \approx 10$ m is an artifact of the model: much of the large-particle material that merely falls near the hypothesized initial position. The ratio of these two curves gives the mass-weighted average particle size, varying as a power law from $\sim 3 \mu\text{m}$ at 20 m radius to $0.04 \mu\text{m}$ at 100 km.

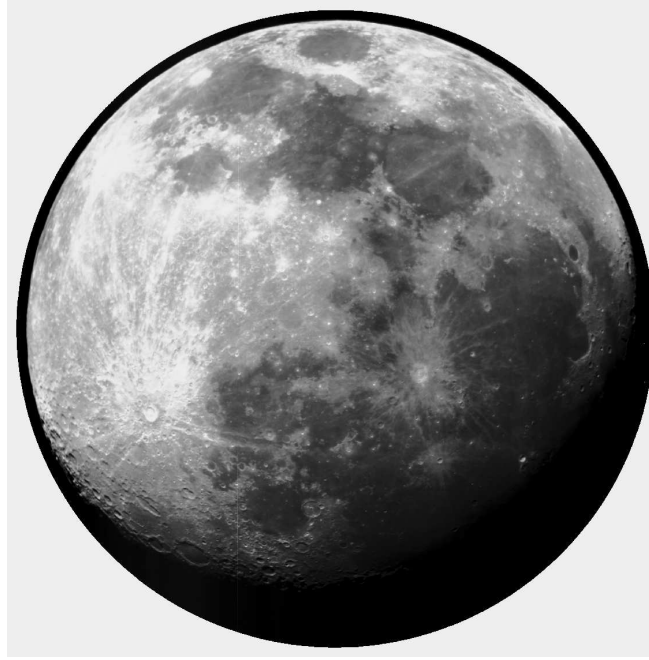
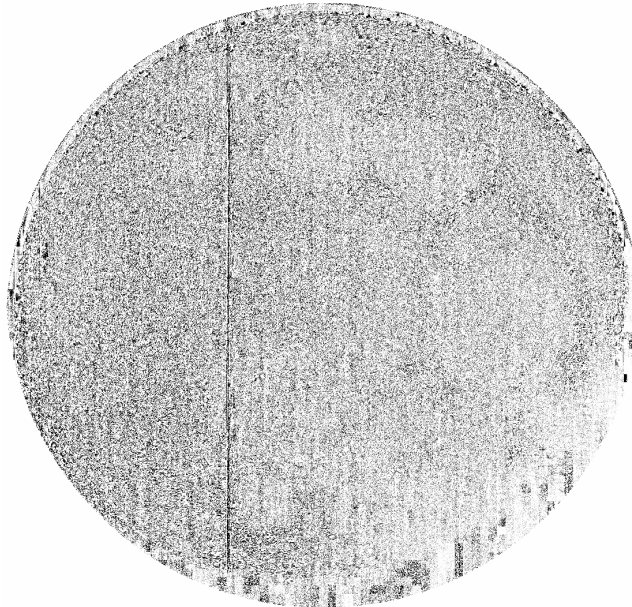


Fig. 4.— Top) Flat-field, dark-corrected but otherwise “raw” image of a typical lunar Near Side image obtained by our robotic imaging monitor. (The image is trimmed to a standard circular region.) Bottom) The difference in signal between the image above and similar one obtained five minutes later. The noise in the residual signal is essentially at the photon shot-noise limit. Because of a slight error in the photometric calibration between the two images there is a very slight ghost of high-contrast global features, especially Imbrium, Humorum and the eastern maria. Note that even bright smaller features e.g., Tycho left and below center, are subtracted nearly identically. Even subtle features not apparent in the image above e.g., an image column acting slightly non-linearly, just left of center, becomes readily apparent. There are also errors along the lunar limb due to the rapid gradient in signal level.



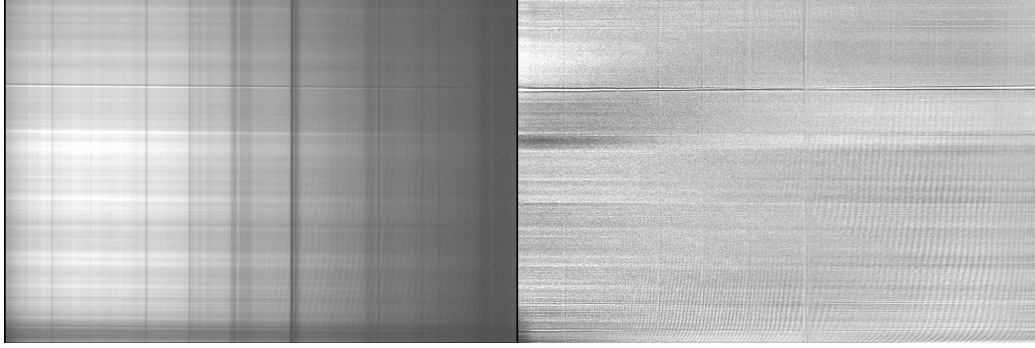


Fig. 5.— **a)** Left: spectrum of an 8-arcmin slit intersecting Aristarchus (bright streak just above center) and extending over Oceanus Procellarum, and covering wavelengths 5500-10500Å, taken by the MDM 2.4-meter telescope; **b)** Right: the residual spectrum once a model consisting of the outer product the one-dimensional average spectrum from Figure 3a times the one-dimensional albedo profile from Figure 3a. The different spectral reflectance of material around Aristarchus is apparent (at a level of about 7% of the initial signal), with r.m.s. deviations of about 0.5%, dominated by interference fringing in the reddest portion, which can be reduced.

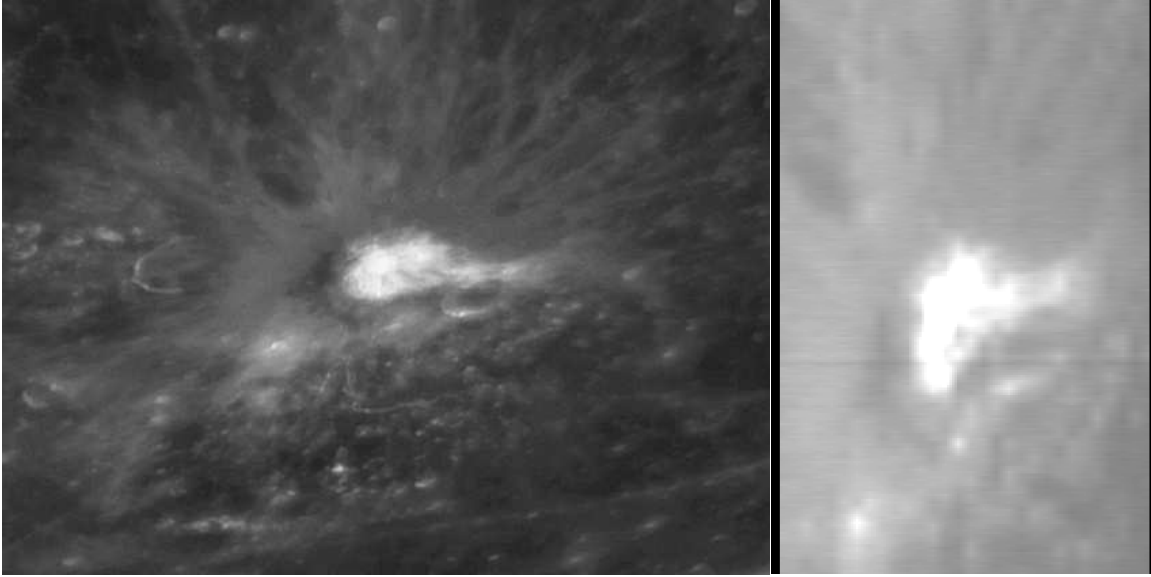


Fig. 6.— **a)** Left: a B-band image of the region around Aristarchus; **b)** Right: an image of Aristarchus in a 3Å-wide centered near 6000Å, constructed by taking a vertical slice through Figure 3a and other exposures from the same sequence of spectra scanning the surface. Any such band between 5500Å and 10500Å can be constructed in the same manner, with resolution of about 1km and 3Å.

Table 1. Summary of Basic Experimental/Observational Techniques Detailed Here

Goal	Detection Method	Channel	Advantages	Difficulties
Map of TLP activity	Imaging monitor, entire nearside, ~ 2 km resolution.	optical	comprehensive schedulability; more sensitive than human eye	limited resolution
Polarimetric study of dust	Compare reflectivity in two monitors with perpendicular polarizers	optical	easy to schedule; further constrains dust behavior	requires use of two monitors
Changes in small, active areas	Adaptive optic imaging, ~ 100 m resolution	$0.95\mu\text{m}$, etc.	“on demand” given good conditions	undemonstrated, depends on seeing; covers ~ 50 km diameter maximum
	“Lucky Imaging,” ~ 200 m resolution	$0.95\mu\text{m}$, etc.	on demand given good conditions	low duty cycle, depends on seeing
	<i>Hubble Space Telescope</i> , ~ 100 m resolution	$0.95\mu\text{m}$, etc.	on demand given advanced notice	limited availability; low efficiency
	<i>Clementine/LRO/Chandrayaan-1</i> imaging, ~ 100 m resolution	$0.95\mu\text{m}$, etc.	existing or planned survey	limited epochs; low flexibility
	<i>LRO/Kaguya/Changé-1</i> imaging, higher resolution	$0.95\mu\text{m}$, etc.	existing or planned survey	limited epochs; low flexibility
TLP spectrum	Scanning spectrometer map, plus spectra taken during TLP event	NIR, optical	may be best method to find composition & TLP mechanism	requires alert from TLP image monitor; limited to long events
Regolith hydration measurement	NIR hydration bands seen before vs. after TLP in NIR imaging	$2.9, 3.4\mu\text{m}$	directly probe regolith/water chemistry; may detect water	requires alert from monitor and flexible scheduling
	Scanning spectrometer map, then spectra taken soon after TLP	$2.9, 3.4\mu\text{m}$	directly probe regolith/water chemistry; may detect water	requires alert from monitor and flexible scheduling
Relationship between TLPs & outgassing	Simultaneous monitoring: ^{222}Rn α particles by <i>Kaguya</i> & optical TLPs	^{222}Rn α & optical	refute/confirm TLP/outgassing correlation; find outgassing loci	optical monitor only covers nearside; more monitors better

Table 1—Continued

Goal	Detection Method	Channel	Advantages	Difficulties
Subsurface water ice	Penetrating radar from Earth	~ 430 MHz	directly find subsurface ice with existing technique	ice signal is easily confused with others
	Penetrating radar from lunar orbit	~ 300 MHz	better resolution; deeper than neutron or gamma probes	ice signal is easily confused; more expensive
	Surface radar from lunar orbit	>1 GHz	better resolution; study TLP site surface changes	redundant with high resolution imaging?
High resolution TLP activity map	Imagers at/near L1, L2 points covering entire Moon, at 100 m resolution	optical	map TLPs with greater resolution & sensitivity, entire Moon	expensive, but could piggyback on communications network
Comprehensive ^{222}Rn α particle map	Two ^{222}Rn α detectors in polar orbits 90° apart in longitude	^{222}Rn α	map outgassing events at full sensitivity	expensive; even better response with 4 detectors
Comprehensive map of outgas components	Two mass spectrometers in adjacent polar orbits	ions & neutrals	map outgassing events & find composition	expensive; even better with more detectors

Note. — In situ, surface experiments: we refer the reader to work in preparation by AEOLUS collaboration. All methods are Earth-based remote sensing unless specified otherwise. Abbreviations used: TLP = transient lunar phenomena, NIR = near infrared